Probabilistic Engineering Mechanics 79 (2025) 103718

Contents lists available at ScienceDirect

Probabilistic Engineering Mechanics

journal homepage: www.elsevier.com/locate/probengmech

Explicit closed-form solution for the evolutionary power spectral density function of the stochastic response of structures subjected to artificial accelerograms consistent with pulse-like ground motions

Federica Genovese [a,*], Giuseppe Muscolino [b]

[a] Department of Architecture and Territory, University Mediterranea of Reggio Calabria, Italy
[b] Department of Engineering, University of Messina, Italy

ARTICLE INFO

Keywords:
Stochastic analysis
Fully non-stationary processes
Evolutionary power spectral density function
Pulse-like accelerograms
Non-geometric spectral moments

ABSTRACT

The near-fault pulse-like ground motions are of great practical interest in seismic engineering. In fact, they tend to cause more serious damage to some types of structures than ordinary ground motions. However, the limited availability of pulse-like records significantly constrains studies involving the randomness of ground motion, such as reliability analysis. To address the scarcity of records, ground motion simulation methods should be used. In the literature, the most efficient one, according to the theory of random processes, is based on the generation of artificial accelerograms as samples of fully non-stationary Gaussian processes. By operating in this way, it is possible to reproduce the typical characteristics of recorded time histories, with both temporal and spectral non-stationarities, which fill the absence of available actual data. In this framework, the authors recently proposed a new model of the *evolutionary power spectral density* (*EPSD*) function to generate artificial accelerograms in such a way that a given target accelerogram can be considered as one of its own samples. The *EPSD* function can be simply evaluated once the frequency of peaks, the zero-level up-crossings, and the total energy of the target accelerogram are determined. This approach, previously applied to the case of ordinary accelerograms, is here extended to pulse-like ones. To effectively achieve this extension, some measures must be taken in the definition of the modulating function and the sub-processes that characterize the *EPSD* function.

In this study, once the way to define the *EPSD* function of the input process is described, a procedure to evaluate in explicit closed form the *EPSD* function of the output process, in terms of displacements and velocities of the structural response, is proposed. Finally, the statistics of the structural response are evaluated, and a reliability analysis is performed in order to demonstrate the accuracy and efficiency of the proposed formulation.

1. Introduction

The first step of structural engineering entails accurately establishing the structural model and determining the associated applied loads. In the framework of seismic engineering, addressing the correct characterization of ground motion acceleration is crucial for the design of structures in seismic risk areas. Earthquake excitation is typically defined through response spectra or, more realistically, by a set of earthquake ground-motion acceleration time-histories, referred to in the literature as accelerograms. Ground motions recorded near a fault rupture (known as near-fault accelerograms) are often different from those recorded relatively far from it (referred to as far-fault or ordinary accelerograms).

Furthermore, the near-fault accelerograms sometimes show high-amplitude velocity pulses, occurring primarily in the fault-normal direction. These accelerograms are usually called pulse-like. It follows that, in the case of pulse-like accelerograms, most of the energy caused by the rupture arrives, near the epicentre, in one burst at the beginning [1]. Unlike ordinary accelerograms, the near-fault pulse-like accelerograms have their energy concentrated in a long-period pulse that can cause considerable damage to flexible structures [1,2]. Moreover, in comparison to far-field seismic records, ground motions characterized by pulse-like features can impose significant displacement demands on structures, elevating the risk of earthquake-induced collapse. This heightened risk is attributed to the fact that structures exposed to pulse-like ground motions must dissipate considerable seismic energy

* Corresponding author.
E-mail addresses: federica.genovese@unirc.it (F. Genovese), giuseppe.muscolino@unime.it (G. Muscolino).

https://doi.org/10.1016/j.probengmech.2024.103718
Received 8 June 2024; Received in revised form 30 October 2024; Accepted 9 December 2024
Available online 10 December 2024

within a relatively short time frame [3]. For these reasons, the pulse-like accelerograms have recently garnered increasing attention.

Several papers have been devoted to the identification of the main parameters of pulse-like accelerograms such as peak ground velocity, pulse period, pulse location, and the number of pulses. To identify and characterize pulses in near-fault forward-directivity ground motions, Mukhopadhyay and Gupta [4] proposed, as indicator, the velocity pulse between two consecutive zero crossings, Vats and Basu [5] proposed a time series-based algorithm that detects the dominant pulse orientation, Chang et al. [6] applied the wavelet packet transform to classify velocity pulses into acceleration and non-acceleration pulses, Chang et al. [7] enhanced the study by incorporating a moving-average filtering method and adopted the relative energy as the pulse indicator, Chen et al. [8] proposed a generalized continuous wavelet transform method for multi-pulse ground motion identification. Alternative signal processing techniques, including the Hilbert–Huang transform [9], variational mode decomposition [10], and empirical Fourier decomposition [11], have been applied to categorize and describe pulse-like ground motions.

It is also widely recognized that the accelerations resulting from intense seismic activity exhibit a stochastic nature. Moreover, examinations of recorded accelerograms have demonstrated that the ground motion accelerations exhibit variations over time in both their intensity and frequency contents. The temporal non-stationarity is related to the time variation of the cumulative intensity (energy) function [12,13], while the spectral non-stationarity is related to the time variation of the number of zero-level up-crossings and peaks [12,14,15]. It follows that recorded accelerograms can be viewed as samples of fully non-stationary zero-mean Gaussian processes, which are characterized by the *Evolutionary Power Spectral Density* (*EPSD*) function [16,17]. Recently, the authors proposed a new model of the one-sided *EPSD* function to generate artificial accelerograms, in such a way that a recorded accelerogram, assumed as target one, can be considered as one of its own samples [18,19]. In this model, the *EPSD* function can be simply evaluated once the frequency of peaks, the zero-level up-crossings, and the total energy of a target accelerogram are determined.

The second step of structural design involves assessing the structural response to predict the safety of structural systems. Within this framework, the maximum absolute peak of stationary or non-stationary stochastic responses offers valuable design insights for various engineering scenarios. Nevertheless, even in the simplest case of an oscillator driven by a zero-mean stationary Gaussian white noise [20,21], the exact probability distribution of the maximum absolute peak of the response is not available. Consequently, several approximate procedures have been proposed to compute statistical characteristics of the response. These approaches result in a probabilistic assessment of structural failure as a function of barrier crossing rates, distribution of peaks, and extreme values. The quantities mentioned above can be computed, particularly for stationary input processes, using the well-known *Spectral Moments* (*SM*s) introduced by Vanmarcke [22].

In the context of stationary stochastic response processes, *SM*s are defined as the geometric moments of the one-sided *Power Spectral Density (PSD)* function associated with the response process. The assessment of these *SM*s is crucial for the approximate reliability evaluation of linear structural systems subjected to stochastic excitations [23].

The application of spectral methods to non-stationary random processes is more challenging than for stationary processes. Specifically, the geometric approach fails for non-stationary processes [24,25]. In response to this challenge, Di Paola [24] introduced the *Pre-Envelope Covariances* (*PEC*s) as the covariances of structural systems subjected to a complex random process, known as the pre-envelope process, in such a way that the complex input and output stochastic processes only exhibit power in the positive frequency range. However, due to the less intuitive nature of the complex pre-envelope process, Michaelov et al. [26,27] assessed the *PEC*s as a function of the *EPSD* function of the response, referring to them as *Non-Geometric Spectral Moments* (*NGSM*s). It is crucial to note that the *NGSM*s of the response provide more comprehensive information than "conventional" covariances. They have been demonstrated to be more suitable for describing non-stationary processes and can be effectively employed in applications related to structural reliability.

The evaluation of *NGSM*s has been conducted through the integral formulation [26–30]. Alternatively, *NGSM*s have been derived as solutions to sets of first-order linear differential equations, applicable to both white [31] and non-white, uniformly modulated input processes [32–34]. Despite the computational advantages of the differential formulation, it is not widely utilized, and the integral formulation is generally preferred. This preference is attributed to the fact that, in the differential formulation, the complex input–output covariances, requiring the Hilbert transform of both input and output, are necessary to define the imaginary part of the complex pre-envelope input process. Furthermore, in the integral formulation framework, it is widely acknowledged that the *Time–Frequency Varying Response* (*TFR*) function [35], also called *Evolutionary Frequency-Response function* [21], holds a central role in assessing the statistics of linear structural systems subjected to non-stationary stochastic excitations. Utilizing the *TFR* function enables the derivation of explicit closed-form solutions for the *EPSD* function of the response. In this context, the *EPSD* function of the response of structures subjected to fully or uniformly modulated non-stationary stochastic processes has been mainly derived by applying the pole-residue method [30,36–40]. An alternative approach based on the explicit closed form evaluation of the *TFR* vector function of classically damped structural systems has been proposed by Muscolino and Alderucci [41]. This approach, which requires the solution of dummy differential equations subjected to simple analytical forcing functions, has been extended afterward to non-classically damped structures [42,43], and to the case of multi-correlated fully non-stationary input [44].

The final step of structural design is to predict the safety of structures. In the framework of stochastic dynamics the main purpose is to evaluate the probability of success or its complement to one, that is the probability of failure. The probability of success is defined as the probability that a quantity of interest, closely related to the displacement and velocity statistics of the structural response, does not exceed a given threshold. To do this, analytical reliability functions have been introduced in the literature [45–50]. By means of these functions, it is possible to evaluate the probability of success in approximate form through very simple relationships, once the *NGSM*s of the response have been evaluated.

In this paper, a procedure for generating fully non-stationary ground motions ensuring energy compatibility with both pulse-like and ordinary recorded accelerograms is first described. The proposed procedure can be viewed as an extension to pulse-like accelerograms of the one recently proposed by the authors in Refs. [18,19], before applied exclusively to ordinary accelerograms. Indeed, in Ref. [18] the modulating function, necessary for the complete definition of the *EPSD* function, was obtained by solving an optimization problem, here avoided. Furthermore, in Ref. [19] only the accelerograms recorded on rock deposits were analyzed; consequently, only the case of uniformly modulated zero-mean Gaussian non-stationary processes was studied. In this paper the more general case of accelerograms recorded on soft soil deposits is analyzed. This extension entails dividing the target accelerogram into multiple time intervals, each with at least one zero level up-crossing and peak, and providing a closed form expression for the modulating function, which depends on the total intensity and on the strong motion duration of the selected recorded accelerogram. It follows that for these accelerograms, the correct stochastic modelling is the fully non-stationary zero-mean Gaussian non-stationary process. It should be emphasized that, especially for pulse-like accelerograms, the division into time intervals is determined by the slope changes variations of the cumulative zero-level up-crossings function, assessing a *PSD* function for each of these time intervals into which the target motion has been subdivided.

Once the *EPSD* function associated with selected recorded accelerogram is determined, the second step involves the evaluation, in explicit closed form, of the *EPSD* function of the output, in terms of displacements and velocities of the structural response of classically damped structural systems. It can be noted that, unlike the formulation in Ref. [41], where explicit form solutions of the *EPSD* function of the response were proposed for modulating functions presented in the literature (Shinozuka and Sato [51], Jennings et al. [52], Spanos and Solomos [53], Hsu and Bernard [54], and Conte and Peng [14]), the closed-form solution presented in this paper is derived for the energy-compatible modulating function proposed by Genovese et al. [19], developed by analysing recorded accelerograms.

In order to verify the versatility of the proposed approach, the *NGSMs* of four oscillators subjected to both ordinary and pulse-like recorded accelerograms are evaluated and compared with the *Monte Carlo Simulation* (*MCS*). Then, for a multi-degree of freedom system, the mean value of the largest peak of structural response is evaluated by the proposed approach, adopting the reliability function introduced by Corotis et al. [45], and compared with *MCS*.

2. Preliminary definitions

2.1. Equations governing the motion

Let us consider a linear quiescent *N-degree-of-freedom* (*N-DOF*) classically damped structural system subjected to seismic ground motion acceleration, $\ddot{U}_g(t)$, whose dynamic behaviour is governed by the following equation of motion:

$$\mathbf{M}\ddot{\mathbf{u}}(t) + \mathbf{C}\dot{\mathbf{u}}(t) + \mathbf{K}\mathbf{u}(t) = -\mathbf{M}\boldsymbol{\tau}\ddot{U}_g(t) \tag{1}$$

where $\mathbf{M}$, $\mathbf{C}$, and $\mathbf{K}$ are the $(N \times N)$ mass, damping, and stiffness matrices of the structure; $\boldsymbol{\tau}$ is the N array listing the influence coefficients; $\mathbf{u}(t)$ is the $(N \times 1)$ vector of displacements, having for i-th element $u_i(t)$ and a dot over a variable denotes differentiation with respect to time. Under the assumption of classically damped system, the equation of motion can be decoupled by applying the modal analysis. Therefore, let introduce the modal coordinate transformation:

$$\mathbf{u}(t) = \boldsymbol{\Phi}\,\mathbf{q}(t) = \sum_{j=1}^{m} \boldsymbol{\phi}_j\, q_j(t) \quad \Rightarrow u_i(t) = \sum_{j=1}^{m} \phi_{ij}\, q_j(t) \tag{2}$$

In Eq. (2), the modal matrix $\boldsymbol{\Phi} = [\,\boldsymbol{\phi}_1 \quad \boldsymbol{\phi}_2 \quad \dots \quad \boldsymbol{\phi}_m\,]$, of order $N \times m$, collects the m eigenvectors $\boldsymbol{\phi}_j$ normalized with respect to the mass matrix $\mathbf{M}$, solutions of the following eigenproblem:

$$\mathbf{K}^{-1}\mathbf{M}\boldsymbol{\Phi} = \boldsymbol{\Phi}\,\boldsymbol{\Omega}^{-2}; \quad \boldsymbol{\Phi}^T\mathbf{M}\boldsymbol{\Phi} = \mathbf{I}_m \tag{3}$$

where $\boldsymbol{\Omega}$ is a diagonal matrix listing the undamped natural circular frequency ω_j, $\mathbf{I}_m$ is the identity matrix of order m and the superscript T denotes the transpose operator.

Once the modal matrix $\boldsymbol{\Phi}$ is evaluated, by applying the coordinate transformations in Eq. (2) to Eq. (1), the following set of decoupled second order differential equations is obtained:

$$\ddot{\mathbf{q}}(t) + \boldsymbol{\Xi}\dot{\mathbf{q}}(t) + \boldsymbol{\Omega}^2\mathbf{q}(t) = -\boldsymbol{\Phi}^T\mathbf{M}\boldsymbol{\tau}\,\ddot{U}_g(t) \tag{4}$$

in which $\boldsymbol{\Xi}$ is the generalized damping matrix given by:

$$\boldsymbol{\Xi} = \boldsymbol{\Phi}^T\mathbf{C}\boldsymbol{\Phi} \tag{5}$$

For classically damped structures the modal damping matrix $\boldsymbol{\Xi}$ is a diagonal matrix listing the quantities $2\xi_j\omega_j$, being ξ_j the modal damping ratio. It follows that the j-th differential Eq. (4) can be written as:

$$\ddot{q}_j(t) + 2\xi_j\omega_j\dot{q}_j(t) + \omega_j^2 q_j(t) = p_j\ddot{U}_g(t), \qquad j = 1, 2, \dots, m; \tag{6}$$

where p_j is the so-called j-th participation factor, that can be evaluated as:

$$p_j = -\,\boldsymbol{\phi}_j^T\,\mathbf{M}\,\boldsymbol{\tau} \tag{7}$$

2.2. Seismic excitation as a fully non-stationary zero-mean Gaussian process

In this paper, a selected recorded accelerogram, of time duration D, is assumed as target one, $\ddot{u}_g^{(T)}(t)$. It is deemed to be representative of the seismic hazard at the site of interest. It is widely recognized that the earthquake-induced ground motion recorded accelerations can be considered samples of zero-mean Gaussian stochastic processes which present non-stationarity in both time and frequency domains. To capture both variations, recently, the authors in Refs. [18,19] proposed a new model in which the variation of the intensity of the target accelerogram, $\ddot{u}_g^{(T)}(t)$, is captured by introducing an appropriate *modulating function*, while the non-stationarity in frequency is captured by introducing a sum of stationary sub-processes, each acting within a well-defined time window. According to this formulation, the mono-correlated zero-mean Gaussian random process $\ddot{U}_g(t)$, modelling the target accelerogram, $\ddot{u}_g^{(T)}(t)$, is defined as the product of a real non-negative deterministic *modulating function* $a(t)$ and the sum of stationary zero-mean Gaussian filtered sub-processes, $X_k(t)$, that is:

$$\ddot{U}_g(t) = a(t)\sum_{k=1}^{n} X_k(t)\ \mathbb{W}(t_{k-1}, t_k) \tag{8}$$

where $\mathbb{W}(t_{k-1}, t_k)$ is a window function defined as follows:

$$\mathbb{W}(t_{k-1}, t_k) = \begin{cases} 1, & t_{k-1} \le t < t_k \\ 0, & t < t_{k-1} \ \text{ and } \ t \ge t_k \end{cases} \tag{9}$$

The *modulating function* $a(t)$, according to the formulation proposed by Genovese et al. [19], is herein defined as:

$$a(t) = a_0 \times \left[\frac{t^2}{t_{a_1}^2}\mathbb{W}(0, t_{a_1}) + \mathbb{W}(t_{a_1}, t_{a_2}) + \exp\left(-\varepsilon_0\left(t - t_{a_2}\right)\right)\mathbb{W}(t_{a_2}, D)\right] \tag{10}$$

where:

$$\varepsilon_0 = \frac{10}{(D - t_{a_2})} \tag{11}$$

In Eq. (10), D is the final time of the recorded accelerogram, while $t_{a_s}\,(s = 1, 2)$ are time instants into which the *modulating function* is subdivided. The two time instants $t_{a_s}\,(s = 1, 2)$ can be selected as a function of the temporal parameters defining the strong motion duration of a target motion. This parameter, rather than the duration of the entire time history D, is considered crucial for identifying the portion of the record where the amplitude of ground motion could potentially cause damage to engineering structures.

Several definitions of strong motion duration have been proposed in the literature, with the commonly used significant duration [55] defined as the interval of time over which a percentage of the total intensity is accumulated. Usually, this range is considered to be between 5% and 95% ($t_{5\text{-}95}$) or between 5% and 75% ($t_{5\text{-}75}$) of the total intensity of the target accelerogram I_0, defined as:

$$I_0 = \int_0^D \left[\ddot{u}_g^{(T)}(t)\right]^2 \mathrm{d}t \tag{12}$$

Note that despite the presence of window functions, the *modulating function* introduced in Eq. (10) is a continuous function in the time interval $0 \le t \le D$, although piecewise defined. Finally, in Eq. (10), the

dimensionless coefficient a_0 is introduced so that the artificial accelerograms possess, in mean, the same total intensity I_0 of the recorded accelerogram. This coefficient is evaluated in closed form as [19]:

$$a_0 = \sqrt{I_0 \Big/ \left[t_{a_2} - \frac{4}{5}t_{a_1} + \frac{(D - t_{a_2})}{20}\right]}. \tag{13}$$

In order to capture the frequency variation of the selected recorded accelerogram, assumed as target one, the frequency variation of the stochastic process $\ddot{U}_g(t)$ is obtained by dividing the overall duration of target accelerogram D into n contiguous time intervals of amplitude $\Delta T_k = t_k - t_{k-1}$. These time intervals are chosen in such a way as to capture the variation of the number of zero-level up-crossings of the target accelerogram, which are closely linked to its variation of the frequency content [18]. Note that, especially for pulse-like accelerograms, the division into time intervals must be determined by the slope changes of the cumulative zero-level up-crossings function. Furthermore, to avoid the superposition of two discontinuities, which could lead to numerical errors, it is necessary to select $t_k \neq t_{a_s}$ and also $t_{k-1} \neq t_{a_s}$. Then, introducing in each time interval a stationary zero-mean Gaussian filtered sub-process, $X_k(t)$, the one-sided *evolutionary power spectral density* (*EPSD*) function of the zero-mean Gaussian fully non-stationary process $\ddot{U}_g(t)$, introduced in Eq. (8), can be written as [18]:

$$G_{\ddot{U}_g}(\omega, t) = a^2(t) \sum_{k=1}^{n} \mathbb{W}(t_{k-1}, t_k) G_{X_k}(\omega) = a^2(t) \widetilde{G}_{\ddot{U}_g}(\omega, t) \tag{14}$$

where $G_{X_k}(\omega)$ is the one-sided *PSD* function of the kth stationary sub-process $X_k(t)$, and

$$\widetilde{G}_{\ddot{U}_g}(\omega, t) = \sum_{k=1}^{n} \mathbb{W}(t_{k-1}, t_k) G_{X_k}(\omega) = \sum_{k=1}^{n} \widetilde{G}_{\ddot{U}_{g,k}}(\omega, t) \tag{15}$$

with

$$\widetilde{G}_{\ddot{U}_{g,k}}(\omega, t) = \mathbb{W}(t_{k-1}, t_k) G_{X_k}(\omega) \tag{16}$$

Note that due to the presence of windows functions, the one-sided *EPSD* function defined in Eq. (14) presents discontinuity of the first kind at time instant $t = t_k, k = 1, 2, \ldots, n$. Indeed, in each time interval $[t_{k-1}, t_k)$ the *PSD* function $G_{X_k}(\omega)$ of the stationary sub-process $X_k(t)$ is independent from the previous and following ones. It is herein assumed that the sub-process $X_k(t)$ is characterized by the following one-sided *PSD* function:

$$G_{X_k}(\omega) = \beta_k \left(\frac{\omega^2}{\omega^2 + \omega_{H,k}^2}\right)\left(\frac{\omega_{L,k}^4}{\omega^4 + \omega_{L,k}^4}\right) G_k^{(CP)}(\omega) \tag{17}$$

where $\omega_{L,k}$ and $\omega_{H,k}$ represent the k-th frequency control of the second order low-pass and first order high-pass Butterworth filters, respectively, and $G_k^{(CP)}(\omega)$ is a unimodal one-sided *PSD* function having unitary area [18]:

$$G_k^{(CP)}(\omega) = \frac{\rho_k}{\pi}\left[\frac{1}{\rho_k^2 + (\omega + \Omega_k)^2} + \frac{1}{\rho_k^2 + (\omega - \Omega_k)^2}\right] \tag{18}$$

The parameters ρ_k and Ω_k introduced in Eq. (18) represent measures of the frequency bandwidth and of the predominant circular frequency of the kth filtered stationary process, respectively. The coefficient β_k, introduced in Eq. (17), ensures that the sub-process $X_k(t)$ possesses unitary variance, i.e. $\sigma_{X_k}^2 = 1$, and can be evaluated as:

$$\beta_k = \frac{2\,\overline{a}_k \overline{b}_k \left(\omega_{H,k}^4 + \omega_{L,k}^4\right)}{\omega_{L,k}^3 (\overline{c}_k + \overline{d}_k + \overline{e}_k)} \tag{19}$$

The coefficients appearing in the closed form expression of Eq. (19) can be calculated as:

$$\begin{aligned}
\overline{a}_k &= \left(\rho_k^2 + \Omega_k^2\right)^4 + 2\left(\rho_k^4 - 6\rho_k^2\Omega_k^2 + \Omega_k^4\right)\omega_{L,k}^4 + \omega_{L,k}^8 \\
\overline{b}_k &= \rho_k^4 + 2\rho_k^2\left(\Omega_k^2 - \omega_{H,k}^2\right) + \left(\Omega_k^2 + \omega_{H,k}^2\right)^2 \\
\overline{c}_k &= -2\,\overline{a}_k\,\rho_k\,\omega_{H,k}\,\omega_{L,k}\left(\rho_k^2 + \Omega_k^2 - \omega_{H,k}^2\right) \\
\overline{d}_k &= \Big[\left(\rho_k^2 + \Omega_k^2\right)^2\left(\rho_k^4 - 6\rho_k^2\Omega_k^2 + \Omega_k^4 + \omega_{L,k}^4\right) \\
&\quad - \omega_{H,k}^2\left(\rho_k^2 - \Omega_k^2\right)\left(\left(\rho_k^2 + \Omega_k^2\right)^2 + \omega_{L,k}^4\right)\Big]\,2\omega_{L,k}\left(\omega_{H,k}^4 + \omega_{L,k}^4\right) \\
\overline{e}_k &= \sqrt{2}\,\overline{b}_k\,\rho_k \\
&\quad \times \Big\{\omega_{L,k}^2\left(\omega_{H,k}^2 - \omega_{L,k}^2\right)\left(\omega_{L,k}^4 + \rho_k^4 - 2\rho_k^2\Omega_k^2 - 3\Omega_k^4\right) \\
&\quad + \left(\omega_{H,k}^2 + \omega_{L,k}^2\right)\left[\rho_k^6 + \Omega_k^6 + 3\Omega_k^2\rho_k^2\left(\rho_k^2 + \Omega_k^2\right) + \omega_{L,k}^4\left(\rho_k^2 - 3\Omega_k^2\right)\right]\Big\}.
\end{aligned} \tag{20}$$

So operating, the fully non-stationary stochastic process $\ddot{U}_g(t)$ defined in Eq. (8) is able to capture simultaneously the time-varying intensity and the time-varying frequency content of the target accelerogram $\ddot{u}_g^{(T)}(t)$ although its single sub-processes are individually *uniformly modulated*. According to Muscolino et al. [18], the control frequencies of the kth pair of Butterworth filters within the time interval $[t_{k-1}, t_k)$ are given by $\omega_{H,k} = 0.1\ \Omega_k$ and $\omega_{L,k} = \Omega_k + 0.8\ \rho_k$. The predominant circular frequency and the circular frequency bandwidth can be evaluated, respectively, as:

$$\Omega_k \cong \frac{2\,\pi\,N_{0,k}^+}{\Delta T_k} \tag{21}$$

$$\rho_k \cong \frac{\pi\,N_{0,k}^+}{2\Delta T_k}\left[\pi - 2\frac{N_{0,k}^+}{P_k}\right] \tag{22}$$

where $N_{0,k}^+$ and P_k are the number of zero-level up-crossings (i.e., crossings of the time axis with positive slope) and the number of peaks of the target accelerogram $\ddot{u}_g^{(T)}(t)$ in the k-th time interval.

The subdivision of target accelerograms into multiple time intervals represents a crucial point of the proposed approach. This time-domain subdivision must accurately capture changes in the slope of the cumulative zero-level up-crossing functions, ensuring that each interval contains at least one zero-level up-crossing and a peak, as required by Eqs. (21) and (22). Once these intervals are identified, a one-sided *PSD* function is then computed using Eq. (17).

2.3. Non-geometric spectral moments

For non-stationary processes, characterized by the one-sided *EPSD* function, the so-called *Non-Geometric Spectral Moments* (*NGSMs*) introduced by Michaelov et al. [26,27] play a fundamental role in the evaluation of structural safety. For linear classically damped structural systems subjected to mono-correlated stochastic input, the r-th *NGSM*, $\lambda_{r,u_i}(t)$ ($r = 0,1,2$), of the i-th nodal response, $u_i(t)$, can be evaluated as a function of *modal cross-NGSM* $p_b\,p_e\,\lambda_{r,be}(t)$ ($b, e = 1, \ldots, m$), by using the following relationships [20,41]:

$$\begin{aligned}
\lambda_{0,u_i}(t) &= \sum_{b=1}^{m}\sum_{e=1}^{m} p_b\,p_e\,\phi_{ib}\,\phi_{ie}\,\lambda_{0,be}(t); \\
\lambda_{1,u_i}(t) &= \sum_{b=1}^{m}\sum_{e=1}^{m} p_b\,p_e\,\phi_{ib}\,\phi_{ie}\,\lambda_{1,be}(t); \\
\lambda_{2,u_i}(t) &= \sum_{b=1}^{m}\sum_{e=1}^{m} p_b\,p_e\,\phi_{ib}\,\phi_{ie}\,\lambda_{2,be}(t).
\end{aligned} \tag{23}$$

It has to be emphasized that the *zero order NGSM*, $\lambda_{0,u_i}(t)$, and the

second order NGSM, $\lambda_{2,u_i}(t)$, are real functions that coincide with the variance of the response in terms of displacement and velocity, respectively; while the *first order NGSM*, $\lambda_{1,u_i}(t)$, is a complex quantity whose imaginary part can be evaluated as the cross-covariance between the displacement response process and the velocity response process of the same *DOF*, while the real part is the cross-covariance between the displacement response process and the response process of the same *DOF* subjected to a non-stationary input whose stationary counterpart is proportional to its Hilbert transform [28,29].

By analysing Eq. (23) it appears that the nodal *NGSM*s can be evaluated once the functions $\lambda_{r,be}(t)$, $r = 0,1,2$, which are the so-called time-dependent modal *NGSM*s, "purged" by p_j factors, are determined. After some algebra, these quantities, which are complex ones, can be evaluated in the time interval $[t_{k-1}, t_k)$, for quiescent structural systems (at time $t = 0$) as follows [41]:

$$\lambda_{r,be}(t) = \sum_{k=1}^{n} \lambda_{r,k,be}(t), \qquad r = 0,1,2 \tag{24}$$

with:

$$\lambda_{0,k,be}(t) = \int_0^\infty Z_b^*(\omega,t) Z_e(\omega,t) \widetilde{G}_{\ddot{U}_{g,k}}(\omega,t)\, \mathrm{d}\omega;$$

$$\lambda_{1,k,be}(t) = -\mathrm{i} \int_0^\infty Z_b^*(\omega,t) \dot{Z}_e(\omega,t) \widetilde{G}_{\ddot{U}_{g,k}}(\omega,t)\, \mathrm{d}\omega; \qquad t_{k-1} \le t < t_k \tag{25}$$

$$\lambda_{2,k,be}(t) = \int_0^\infty \dot{Z}_b^*(\omega,t) \dot{Z}_e(\omega,t) \widetilde{G}_{\ddot{U}_{g,k}}(\omega,t) \mathrm{d}\omega$$

where $\widetilde{G}_{\ddot{U}_{g,k}}(\omega,t)$ is the function defined in Eq. (16). It follows that the "purged" *NGSM* $\lambda_{r,k,be}(t)$, $(r = 0,1,2)$ could present discontinuities of the first kind in each time interval $[t_{k-1}, t_k)$. It follows that the *NGSM*s, given in Eq. (23), could be discontinuous functions too. Indeed, they have to be evaluated taking into account the various time intervals in which the target accelerogram is subdivided. Finally, in writing Eq. (25), for *j*=*b*,*e*, the following positions have been made [41]:

$$Z_j(\omega,t) = \int_0^t h_j(t-\tau) \exp(\mathrm{i}\omega\tau) a(\tau) \mathrm{d}\tau;$$

$$\dot{Z}_j(\omega,t) = \int_0^t \dot{h}_j(t-\tau) \exp(\mathrm{i}\omega\tau) a(\tau) \mathrm{d}\tau \tag{26}$$

where $h_j(t)$ is the impulse response function of the *j*-th modal oscillator defined as follows:

$$h_j(t) = \frac{1}{\overline{\omega}_j} \exp(-\xi_j \omega_j t) \sin(\overline{\omega}_j t); \quad t \ge 0 \tag{27}$$

and $\overline{\omega}_j = \omega_j \sqrt{1-\xi_j^2}$ is the damped circular frequency of the *j*-th oscillator.

It has to be emphasized that the function $Z_j(\omega,t)$ introduced in Eq. (26) is the so-called *modal time–frequency varying response (TFR) function* of the *j*-th modal oscillator ($j = b$,*e*) [21,35,41], and $\dot{Z}_j(\omega,t)$ is its derivative with respect to time. Notice also that, if the *modulating function* is assumed to be equal to the *Heaviside unit step function*, $a(t) = \mathbb{U}(t)$, with $\mathbb{U}(t)$ defined as:

$$\mathbb{U}(t-t_0) = \begin{cases} 0, & t < t_0 \\ 1, & t \ge t_0 \end{cases}; \tag{28}$$

and taking the limit as $t \to \infty$, the first of Eq. (26) leads to:

$$\lim_{t\to\infty} Z_j(\omega,t) = \exp(\mathrm{i}\,\omega\, t) H_j(\omega) \tag{29}$$

where $H_j(\omega)$ is the *frequency response function* of the *j*-th modal oscillator:

$$H_j(\omega) = \frac{1}{\omega_j^2 - \omega^2 + \mathrm{i}\, 2\xi_j \omega_j \omega} \tag{30}$$

3. Stochastic response of linear structural systems

3.1. Explicit closed form solution for the time–frequency varying response function

In this section, explicit closed-form solutions of the modal *TFR* function of the *j*-th oscillator ($j = b$, *e*), defined in Eq. (26), are evaluated. To do this, the function $Z_j(\omega,t)$ introduced in Eq. (26) as a Duhamel's type integral, is here obtained as the solution of dummy oscillators whose motion is governed by the following differential equation with at-rest initial condition [41]:

$$\begin{aligned} \ddot{Z}_j(\omega,t) + 2\xi_j\omega_j\dot{Z}_j(\omega,t) + \omega_j^2 Z_j(\omega,t) &= \exp(\mathrm{i}\omega t) a(t); \\ Z_j(\omega,0) = 0, \quad \dot{Z}_j(\omega,0) &= 0 \end{aligned} \tag{31}$$

Note that this approach appears similar but it is conceptually very different from the pseudo-excitation method proposed by Lin et al. [56], where the *PSD* function of the stationary counterpart of the input appears in the right-hand side of Eq. (31). It follows that the physical dimension of the *TFR* function is totally different from the function derived by applying the pseudo-excitation method. Furthermore, being the *modulating function* $a(t)$ subdivided in three time intervals (see Eq. (10)), the *TFR* function of the *j*-th oscillator, solution of Eq. (31), must be evaluated as the sum of three functions, i.e.:

$$\begin{aligned} Z_j(\omega,t) = Z_j^{(1)}(\omega,t)\, \mathbb{W}(0,t_{a_1}) + Z_j^{(2)}(\omega,t)\, \mathbb{W}(t_{a_1},t_{a_2}) \\ + Z_j^{(3)}(\omega,t)\, \mathbb{W}(t_{a_2},D) \end{aligned} \tag{32}$$

where the functions $Z_j^{(s)}(\omega,t)$, with $s = 1,2,3$, are solution of the following differential equations:

$$\ddot{Z}_j^{(s)}(\omega,t) + 2\xi_j\omega_j\dot{Z}_j^{(s)}(\omega,t) + \omega_j^2 Z_j^{(s)}(\omega,t) = \exp(\mathrm{i}\omega t) a^{(s)}(t). \tag{33}$$

These three differential equations can be solved by imposing on each of them the corresponding *modulating function* and the initial conditions listed below:

$$a^{(1)}(t) = a_0 \left(\frac{t}{t_{a_1}}\right)^2; \qquad Z_j^{(1)}(\omega,0) = 0, \quad \dot{Z}_j^{(1)}(\omega,0) = 0;$$

$$a^{(2)}(t) = a_0; \quad Z_j^{(2)}(\omega,t_{a_1}) = Z_j^{(1)}(\omega,t_{a_1}), \dot{Z}_j^{(2)}(\omega,t_{a_1}) = \dot{Z}_j^{(1)}(\omega,t_{a_1}); \tag{34}$$

$$a^{(3)}(t) = a_0 \exp\left[-\varepsilon_0 (t - t_{a_2})\right]; \qquad \begin{aligned} Z_j^{(3)}(\omega,t_{a_2}) &= Z_j^{(2)}(\omega,t_{a_2}), \\ \dot{Z}_j^{(3)}(\omega,t_{a_2}) &= \dot{Z}_j^{(2)}(\omega,t_{a_2}). \end{aligned}$$

Since the forcing terms are expressed in a simple analytical form, the solutions of Eq. (33) can be pursued in several ways. The first is the Laplace transformation method, which is the most commonly used within the theory of linear systems (see e.g. Ref. [57]). This method, which for the evaluation of the inverse Laplace transformation requires the use of the partial fraction method [58], has recently been applied to evaluate the *TFR* function [40]. However, this method could be cumbersome in the evaluation of poles and residues, especially for linear systems without initial rest conditions and forcing function that modifies the time variation law in various time intervals, as in the case of the modulation function given in Eq. (10). Therefore, an alternative way is adopted in this paper to obtain the *TFR* function. Specifically, the general solution of each of Eq. (33) is evaluated by the combination of the *complementary solution* $Z_{c,j}^{(s)}(\omega,t)$ and the *particular solution* $Z_{p,j}^{(s)}(\omega,t)$ [59]:

$$Z_j^{(s)}(\omega,t)=Z_{\mathrm{p},j}^{(s)}(\omega,t)+Z_{\mathrm{C},j}^{(s)}(\omega,t);\quad s=1,2,3 \tag{35}$$

The first step of the approach adopted here is the evaluation of *particular solutions* of Eq. (33). After very simple algebra it can be proven that the particular solutions of the three differential equations given in Eq. (33) are the following:

$$\begin{aligned}
Z_{\mathrm{p},j}^{(1)}(\omega,t)&=\frac{a_0}{t_1^2}\Big[H_j(\omega)\,t^2-4\big(\mathrm{i}\,\omega+\xi_j\,\omega_j\big)H_j^2(\omega)\,t-2H_j^2(\omega)\\
&\quad+8\big(\mathrm{i}\,\omega+\xi_j\,\omega_j\big)^2H_j^3(\omega)\Big]\exp(\mathrm{i}\omega t),\qquad 0\le t<t_{a_1};\\
Z_{\mathrm{p},j}^{(2)}(\omega,t)&=a_0\,H_j(\omega)\exp(\mathrm{i}\omega t),\qquad t_{a_1}\le t<t_{a_2};\\
Z_{\mathrm{p},j}^{(3)}(\omega,t)&=a_0\,\chi_j(\omega)\exp(-\varepsilon_0(t-t_2))\exp(\mathrm{i}\omega t),\qquad t_{a_2}\le t\le D;
\end{aligned} \tag{36}$$

where the *frequency response function* $H_j(\omega)$ of the j-th modal oscillator is defined in Eq. (30), and:

$$\chi_j(\omega)=\frac{1}{\omega_j^2+2\,\xi_j\omega_j\,\beta(\omega)+\beta(\omega)^2};\quad \beta(\omega)=-\varepsilon_0+\mathrm{i}\omega \tag{37}$$

The *complementary solutions* coincide with the free-vibration responses of Eq. (33) and can be formally written as:

$$Z_{\mathrm{C},j}^{(s)}(\omega,t)=\exp(-\xi_j\omega_j\,t)\left[A_j^{(s)}\cos(\overline{\omega}_j\,t)+B_j^{(s)}\cos(\overline{\omega}_j\,t)\right],\ s=1,2,3 \tag{38}$$

where the constants $A_j^{(s)}$ and $B_j^{(s)}$ may be expressed in terms of the initial conditions, $Z_j^{(s)}(\omega,t_{a_{s-1}})$ and $\dot{Z}_j^{(s)}(\omega,t_{a_{s-1}})$, with at-rest at the initial time $t=0$. After some algebra, evaluated the constants $A_j^{(s)}$ and $B_j^{(s)}$ by imposing the initial conditions for each differential Eq. (33), the *complementary solutions* can be written as [60,61]:

$$\begin{aligned}
Z_{\mathrm{C},j}^{(1)}(\omega,t)&=\frac{a_0}{t_{a_1}^2}\Big\{\Big[8(\mathrm{i}\omega+\xi_j\omega_j)^2H_j^3(\omega)-2H_j^2(\omega)\Big]\Big[\omega_j^2g_j(t)-\mathrm{i}\omega h_j(t)\Big]\\
&\quad+4(\mathrm{i}\omega+\xi_j\omega_j)\,H_j^2(\omega)h_j(t)\Big\},\qquad 0\le t<t_{a_1};\\
Z_{\mathrm{C},j}^{(2)}(\omega,t)&=-\omega_j^2g_j(t-t_{a_1})\,Z_j^{(1)}(\omega,t_{a_1})+h_j(t-t_{a_1})\,\dot{Z}_j^{(1)}(\omega,t_{a_1})\\
&\quad+a_0H_j(\omega)\Big[\omega_j^2g_j(t-t_{a_1})\exp(\mathrm{i}\omega t_{a_1})-\mathrm{i}\omega h_j(t-t_{a_1})\exp(\mathrm{i}\omega t_{a_1})\Big],\\
&\qquad t_{a_1}\le t<t_{a_2};\\
Z_{\mathrm{C},j}^{(3)}(\omega,t)&=-\omega_j^2g_j(t-t_{a_2})\,Z_j^{(2)}(\omega,t_{a_2})+h_j(t-t_{a_2})\,\dot{Z}_j^{(2)}(\omega,t_{a_2})\\
&\quad+a_0\chi_j(\omega)\Big[\omega_j^2g_j(t-t_{a_2})\exp(\mathrm{i}\omega t_{a_2})-\beta(\omega)h_j(t-t_{a_2})\exp(\mathrm{i}\omega t_{a_2})\Big],\\
&\qquad t_{a_2}\le t<D;
\end{aligned} \tag{39}$$

where the function $h_j(t)$ is defined in Eq. (27), while

$$g_j(t)=-\frac{1}{\omega_j^2}\exp(-\xi_j\,\omega_j\,t)\left[\cos(\overline{\omega}_j\,t)+\frac{\xi_j\,\omega_j}{\overline{\omega}_j}\sin(\overline{\omega}_j\,t)\right];\quad t\ge 0 \tag{40}$$

Substituting Eqs. (36) and (39) into Eq. (35), the *general solutions* of Eq. (33) are determined.

3.2. Explicit closed form solution for the one-sided cross-EPSD function

It is well known that, within the framework of stochastic dynamics of structures, the statistical characteristics of a zero-mean Gaussian fully non-stationary stochastic process can be totally determined once its one-sided *EPSD* function is known. Unlike stationary excitations, the *EPSD* function of the response of structures subjected to non-stationary stochastic processes cannot be directly derived from the *EPSD* function of displacements [28,29]. In fact, the following inequalities hold:

$$G_{u_iu_i}(\omega,t)\ne\omega G_{u_iu_i}(\omega,t);\quad G_{u_iu_i}(\omega,t)\ne\omega^2\,G_{u_iu_i}(\omega,t) \tag{41}$$

It has been proven that the one-sided *EPSD* functions of the nodal response, in terms of displacements and velocities, of structural systems subjected to fully non-stationary zero-mean Gaussian processes can be evaluated using the following relationships [21,41]:

$$\begin{aligned}
G_{u_iu_i}(\omega,t)&=\sum_{b=1}^{m}\sum_{e=1}^{m}p_b\,p_e\,\phi_{ib}\,\phi_{ie}\,G_{Z_bZ_e}(\omega,t);\\
G_{u_i\dot{u}_i}(\omega,t)&=\sum_{b=1}^{m}\sum_{e=1}^{m}p_b\,p_e\,\phi_{ib}\,\phi_{ie}\,G_{Z_b\dot{Z}_e}(\omega,t);\\
G_{\dot{u}_i\dot{u}_i}(\omega,t)&=\sum_{b=1}^{m}\sum_{e=1}^{m}p_b\,p_e\,\phi_{ib}\,\phi_{ie}\,G_{\dot{Z}_b\dot{Z}_e}(\omega,t);
\end{aligned} \tag{42}$$

where $G_{Z_bZ_e}(\omega,t)$, $G_{Z_b\dot{Z}_e}(\omega,t)$, and $G_{\dot{Z}_b\dot{Z}_e}(\omega,t)$ are the one-sided modal *cross-EPSD* functions between displacements and velocities of the response of modal oscillators "purged" by p_j factors.

In the case analyzed, the modulating function is governed by three different analytical laws, in three contiguous time intervals, it follows that the one-sided modal *cross-EPSD* functions must be determined as the superposition of three different functions:

$$\begin{aligned}
G_{Z_bZ_e}(\omega,t)&=\mathbb{W}(0,t_{a_1})\,G_{Z_bZ_e}^{(1)}(\omega,t)+\mathbb{W}(t_{a_1},t_{a_2})\,G_{Z_bZ_e}^{(2)}(\omega,t)\\
&\quad+\mathbb{W}(t_{a_2},D)\,G_{Z_bZ_e}^{(3)}(\omega,t);\\
G_{Z_b\dot{Z}_e}(\omega,t)&=\mathbb{W}(0,t_{a_1})\,G_{Z_b\dot{Z}_e}^{(1)}(\omega,t)+\mathbb{W}(t_{a_1},t_{a_2})\,G_{Z_b\dot{Z}_e}^{(2)}(\omega,t)\\
&\quad+\mathbb{W}(t_{a_2},D)\,G_{Z_b\dot{Z}_e}^{(3)}(\omega,t);\\
G_{\dot{Z}_b\dot{Z}_e}(\omega,t)&=\mathbb{W}(0,t_{a_1})\,G_{\dot{Z}_b\dot{Z}_e}^{(1)}(\omega,t)+\mathbb{W}(t_{a_1},t_{a_2})\,G_{\dot{Z}_b\dot{Z}_e}^{(2)}(\omega,t)\\
&\quad+\mathbb{W}(t_{a_2},D)\,G_{\dot{Z}_b\dot{Z}_e}^{(3)}(\omega,t).
\end{aligned} \tag{43}$$

Consequently, the one-sided modal *cross-EPSD* functions present discontinuity of the first kind at time instants $t=t_{a_1}$ and $t=t_{a_2}$. Moreover, the *EPSD* functions that appear on the right side of the previous equation are determined as solution of dummy oscillators defined in Eq. (33). In fact, as the *TFR* functions $Z_j^{(s)}(\omega,t)$ $(s=1,2,3;\ j=b,e)$ of dummy oscillators are evaluated in explicit closed form solution, it is possible to evaluate these *EPSD* functions by very simple analytical relationships [41]:

$$\begin{aligned}
G_{Z_bZ_e}^{(s)}(\omega,t)&=\sum_{k=1}^{n}\mathbb{W}(t_{k-1},t_k)\,Z_b^{(s)*}(\omega,t)\,Z_e^{(s)}(\omega,t)G_{X_k}(\omega);\\
G_{Z_b\dot{Z}_e}^{(s)}(\omega,t)&=\sum_{k=1}^{n}\mathbb{W}(t_{k-1},t_k)\,Z_b^{(s)*}(\omega,t)\,\dot{Z}_e^{(s)}(\omega,t)G_{X_k}(\omega);\quad s=1,2,3\\
G_{\dot{Z}_b\dot{Z}_e}^{(s)}(\omega,t)&=\sum_{k=1}^{n}\mathbb{W}(t_{k-1},t_k)\,\dot{Z}_b^{(s)*}(\omega,t)\,\dot{Z}_e^{(s)}(\omega,t)G_{X_k}(\omega).
\end{aligned} \tag{44}$$

In these equations, $G_{X_k}(\omega)$ is the *PSD* function of the k-th stationary subprocess defined in Eq. (17). Note that for the presence of window functions, the one-sided *EPSD* functions defined in Eq. (44) present discontinuity of the first kind at time instant $t=t_k$, $k=1,2,\ldots,n$, which are combined to the discontinuities present in Eq. (43).

3.3. Non-geometric spectral moments of stochastic response

Once the one-sided modal *cross-EPSD* functions (see Eq. (44)) are determined, the "purged" *NGSMs* in the s-th interval, into which the *modulating function* $a(t)$ is subdivided (see Eq. (10)), are evaluated by

solving the following integrals:

$$\lambda_{0,be}^{(s)}(t) = \int_0^\infty G_{Z_b Z_e}^{(s)}(\omega,t)\mathrm{d}\omega = \sum_{k=1}^{n} \lambda_{0,k,be}^{(s)}(t);$$

$$\lambda_{1,be}^{(s)}(t) = -\mathrm{i}\int_0^\infty G_{Z_b \dot{Z}_e}^{(s)}(\omega,t)\mathrm{d}\omega = \sum_{k=1}^{n} \lambda_{1,k,be}^{(s)}(t); \qquad s=1,2,3 \tag{45}$$

$$\lambda_{2,be}^{(s)}(t) = \int_0^\infty G_{\dot{Z}_b \dot{Z}_e}^{(s)}(\omega,t)\mathrm{d}\omega = \sum_{k=1}^{n} \lambda_{2,k,be}^{(s)}(t),$$

where $\lambda_{r,k,be}^{(s)}(t)$ is evaluated numerically according to Eq. (25) as:

$$\lambda_{0,k,be}^{(s)}(t) = \mathbb{W}(t_{k-1},t_k)\int_0^\infty Z_b^{(s)*}(\omega,t) Z_e^{(s)}(\omega,t) G_{X_k}(\omega)\mathrm{d}\omega;$$

$$\lambda_{1,k,be}^{(s)}(t) = -i\,\mathbb{W}(t_{k-1},t_k)\int_0^\infty Z_b^{(s)*}(\omega,t)\,\dot{Z}_e^{(s)}(\omega,t)\,G_{X_k}(\omega)\mathrm{d}\omega; \tag{46}$$

$$\lambda_{2,k,be}^{(s)}(t) = \mathbb{W}(t_{k-1},t_k)\int_0^\infty \dot{Z}_b^{(s)*}(\omega,t)\dot{Z}_e^{(s)}(\omega,t) G_{X_k}(\omega)\mathrm{d}\omega; \qquad s=1,2,3$$

Finally, the $b-th$, $e-th$ cross "purged" *NGSM* can be evaluated as the sum of the three functions given in Eq. (45) as follows:

$$\lambda_{r,be}(t) = \lambda_{r,be}^{(1)}\left(t\right)\,\mathbb{W}\left(0,t_{a_1}\right) + \lambda_{r,be}^{(2)}\left(t\right)\,\mathbb{W}\left(t_{a_1},t_{a_2}\right) + \lambda_{r,be}^{(3)}\left(t\right)\,\mathbb{W}\left(t_{a_2},D\right); \quad r=0,1,2 \tag{47}$$

Substituting the cross "purged" *NGSM*s into Eq. (23), the nodal *NGSM*s of the classically damped structural system are obtained as follows:

$$\begin{aligned}\lambda_{0,u_i}(t) &= \sum_{b=1}^{m}\sum_{e=1}^{m} p_b\, p_e\, \phi_{ib}\, \phi_{ie} \\ &\times \left[\lambda_{0,be}^{(1)}(t)\mathbb{W}(0,t_{a_1}) + \lambda_{0,be}^{(2)}(t)\mathbb{W}(t_{a_1},t_{a_2}) + \lambda_{0,be}^{(3)}(t)\mathbb{W}(t_{a_2},D)\right];\end{aligned}$$

$$\begin{aligned}\lambda_{1,u_i}(t) &= \sum_{b=1}^{m}\sum_{e=1}^{m} p_b\, p_e\, \phi_{ib}\, \phi_{ie} \\ &\times \left[\lambda_{1,be}^{(1)}(t)\mathbb{W}(0,t_{a_1}) + \lambda_{1,be}^{(2)}(t)\mathbb{W}(t_{a_1},t_{a_2}) + \lambda_{1,be}^{(3)}(t)\mathbb{W}(t_{a_2},D)\right];\end{aligned}$$

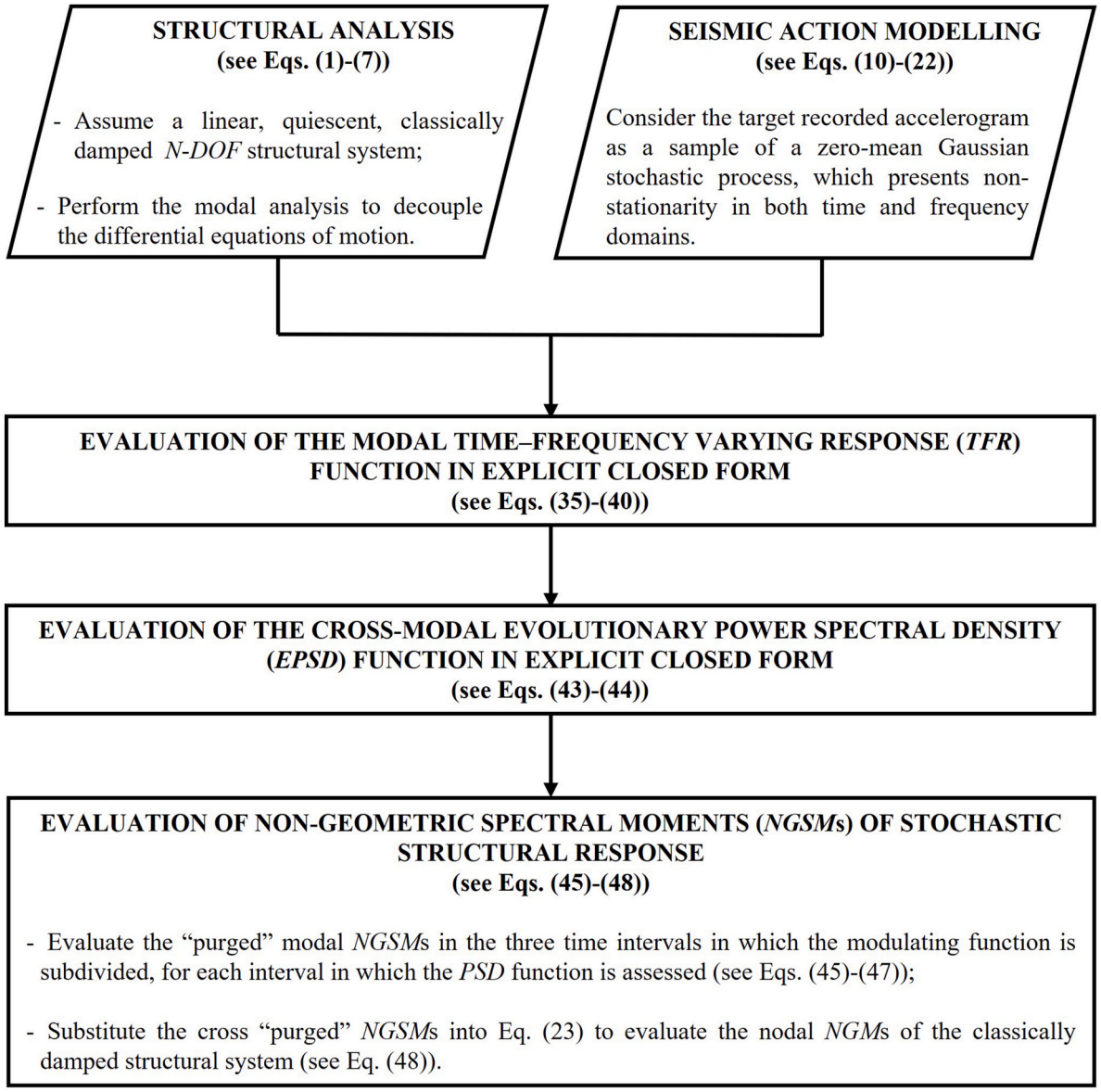

Fig. 1. Flowchart of the proposed procedure for the evaluation of nodal *NGSM*s.

$$\lambda_{2,u_i}(t) = \sum_{b=1}^{m}\sum_{e=1}^{m} p_b\, p_e\, \phi_{ib}\, \phi_{ie} \times \left[\lambda_{2,be}^{(1)}(t)\mathbb{W}(0,t_{a_1}) + \lambda_{2,be}^{(2)}(t)\mathbb{W}(t_{a_1},t_{a_2}) + \lambda_{2,be}^{(3)}(t)\mathbb{W}(t_{a_2},D)\right] \quad (48)$$

For the sake of clarity, the procedure for calculating *NGSMs* is summarised in the flowchart in Fig. 1.

Known the nodal *NGSMs*, it is possible to approximate both the reliability function and the probability of success [45–50].

4. Numerical applications

The purpose of this section is to validate the proposed procedure for the evaluation of the response of linear structural systems subjected to seismic accelerations modeled as fully non-stationary zero mean Gaussian stochastic processes. To this purpose two recorded accelerograms are analyzed: one pulse-like and one ordinary. Then, according to the procedure described in Section 2, the parameters of the *EPSD* functions associated to the two selected recorded accelerograms are evaluated. Subsequently, two sets of artificial accelerograms are generated so that the two target ones can be considered as samples. Finally, the effectiveness of the proposed method is showcased through two numerical applications. The first application involves the analysis of four single-degree-of-freedom (*SDoF*) systems. In the second application a reliability analysis test is performed by evaluating the mean value of the largest peak of the response for a six-story spatial frame. In both applications the results obtained by the proposed procedure are compared with those obtained by using the *Monte Carlo simulation* (*MCS*).

4.1. Target accelerations

In order to generate artificial accelerograms using the *EPSD* model recently introduced by the authors [18,19] and synthesized in section 2.2, two types of near-field ground motions, downloaded from Peer database, have been selected as target accelerograms $\ddot{u}_g^{(T)}(t)$ (see Fig. 2):

- the first horizontal component (HVP225) of ground motion "Imperial Valley-06", recorded in 1979, is pulse-like. It displays distinct pulses in acceleration, velocity, and displacement time histories (see Fig. 2 a,c,e). The recording station, situated at the Holtville Post Office on deep deposits of dense sand with a shear wave velocity $V_{s,30}$ = 202.89 m/s, falls into soil class C according to the European Commission Standard EC8 [62]. The site-source distance is R_{JB} = 5.35 km, and the closest distance to the fault rupture plane is R_{rup} = 7.5 km. The selected motion, with magnitude M_w = 6.53, overall duration D = 37.86 s, sampling step Δt=0.005 s, and peak ground acceleration PGA = 2.53 m/s^2, is characterized by a total intensity I_0 = 5.52783 m^2/s^3 and Arias intensity I_A = 0.885 m/s. The strong motion duration of the target motion is $D_{5\text{-}75}$ = 4.695 s, while the times corresponding to the 5% and 75% of I_0 are respectively t_5 = 4.71 s and t_{75} = 9.405 s. The total number of zero-level up-crossings and of peaks are equal to N_0^+=141 and P_0=330, respectively. For the selected accelerogram, the dimensionless coefficient of Eq. (13), used in the subsequent sections for the evaluation of the energy-compatible modulating function, is equal to a_0 = 0.885 m/s^2;
- the second horizontal component (ELC270) of the 1940 "Imperial Valley-02" ground motion does not contain pulses in the acceleration, velocity or displacement histories (see Fig. 2 b,d,f). The

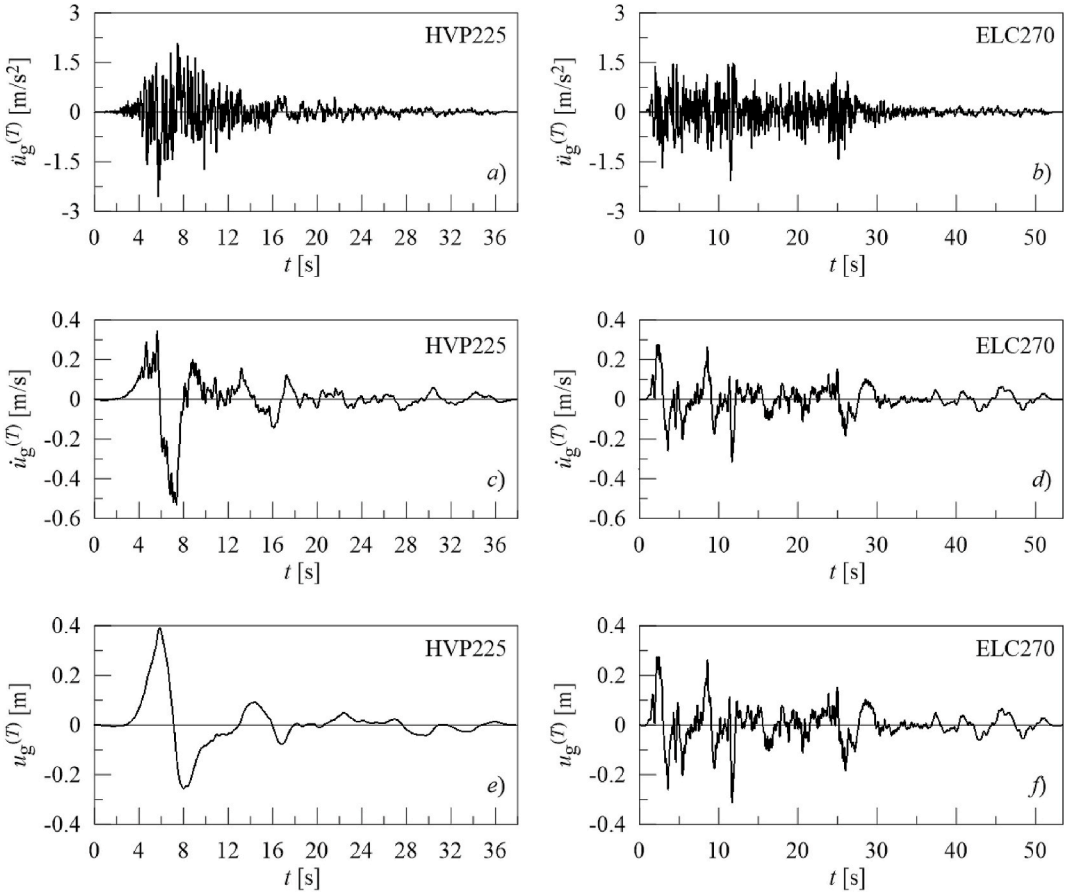

Fig. 2. Time histories of the two target ground motions: (a,b) acceleration; (c,d) velocity, (e,f) displacements. Left column: 1979 Imperial Valley-06 (HVP225) (pulse-like accelerogram); right column: 1940 Imperial Valley-02 (ELC270) (ordinary accelerogram).

recording station, located on deep deposits of dense sand with $V_{s,30} = 213.44$ m/s (soil class C according to EC8), is characterized by a site-source distance $R_{JB} = 6.09$ km and a closest-distance to the fault rupture plane $R_{rup} = 6.09$ km. The selected motion of magnitude $M_w = 6.95$, overall duration $D = 53.45$ s, sampling step $\Delta t = 0.01$ s and peak ground acceleration $PGA = 2.06$ m/s^2, is characterized by a total intensity $I_0 = 7.30$ m^2/s^3 and an Arias intensity $I_A = 1.16$ m/s; the strong motion duration of the target motion is $D_{5\text{-}75} = 17.73$ s while the times corresponding to the 5% and 75% of I_A are respectively $t_5 = 2.15$ s and $t_{75} = 19.88$ s. The total number of zero-level up-crossings and of peaks are equal to $N_0^+ = 145$ and $P_0 = 239$, respectively. The coefficient of Eq. (13), applied in the following sections to assess the energy-compatible modulating function for the ELC270 accelerogram is equal to $a_0 = 0.606598$ m/s^2.

4.2. Generation of artificial accelerograms compatible with target ground motions

In this section, the one-sided *EPSD* function evaluated in Section 2.2 is used for generating samples of fully non-stationary zero-mean Gaussian processes, so that a given target accelerogram can be considered one of its own samples. The fully non-stationary zero-mean Gaussian input process, can be defined as the sum of zero-mean Gaussian uniformly modulated sub-processes $X_k(t)$, defined in contiguous time intervals (see Eq. (14)) and possessing a one-sided *PSD* function $G_{X_k}(\omega)$ with unit variance, multiplied by a modulating function. Consequently, the determination of both the *modulating function* and the fundamental parameters that characterize the *PSD* function of each sub-process is conducted separately.

4.2.1. Evaluation of the PSD function parameters

The one-sided *PSD* function $G_{X_k}(\omega)$ associated with the Gaussian sub-process, $X_k(t)$, depends solely on the count of peaks P_k and zero-level up-crossings $N_{0,k}^+$ occurring during the kth time interval $\Delta T_k = t_k - t_{k-1}$ ($k = 1,2,\ldots,n$) within which the target accelerogram has been subdivided. The procedure proposed by Muscolino et al. [18] is applied herein to the two selected recorded accelerograms, one of which exhibits pulse-like behaviour.

Both accelerograms, recorded as near-fault motions on soft soils, are characterized by a non-linear trend of the cumulative zero-level up-crossing function $N_0^+(t)$, as evident from the analysis of two functions depicted in Fig. 3. To obtain the non-stationary stochastic processes, which include the target accelerograms among their samples, it is necessary to subdivide both target accelerograms into different time intervals, each containing at least one zero-level up-crossing and peak, and then evaluate a one-sided *PSD* function for each time interval into which the target motion has been subdivided. In this numerical application, both accelerograms have been subdivided into five-time regions, identified based on the change in slope of the zero-level up-crossing functions. The selected five-time regions for both target signals are indicated in Fig. 3, filled with different colours, and delineated by dashed black vertical lines.

Fig. 4 shows the one-sided *PSD* functions $G_{X_k}(\omega)$ computed for each of the five time region into which the target signals are subdivided. The same colours are used to highlight which region of the range each one-sided *PSD* function is associated with. Table I and Table II list the parameters useful for their evaluation: t_k, time instants corresponding to the passage from one interval to another; ΔT_k, amplitude of the k-th time interval; $N_{0,k}^+$ and P_k total number of zero-level up-crossings and peaks in the k-th time interval; Ω_k, predominant circular frequency; ρ_k, circular frequency bandwidth; $\omega_{L,k}$ and $\omega_{H,k}$ circular control frequencies of low-pass and high-pass Butterworth filters; β_k, normalizing coefficient.

4.2.2. Energy-compatible modulating functions

The modulating function $a(t)$ is evaluated to be energy compatible. This function, according to Eqs. (10) and (12), in turn depends on the cumulative intensity of the target motion $I_0(t)$ defined as:

$$I_0(t) = \int_0^t \left[\ddot{u}_g^{(T)}(t)\right]^2 \mathrm{d}t \tag{49}$$

The values of the time instants, t_{a_s} ($s = 1, 2$), corresponding to the passage from one interval to another in the piecewise modulating function of Eq. (10) have been assumed to be equal to the time instants characterizing the *strong motion duration* $D_{5\text{-}75}$ of the target accelerogram. Specifically, in Eqs. (10)–(13) have been set $t_{a_1} = t_5$ and $t_{a_2} = t_{75}$ that correspond to the times at which 5% and 75% of the total intensity $I_0(t)$ has been released, respectively.

For the two target accelerograms, the *modulating functions* are shown in Fig. 5 (solid black lines) together with the absolute value of the target motions (grey line) and the trend of the cumulative intensity functions $I_0(t)$. As evident from the trends depicted in Fig. 5, the strong motion duration region of the pulse-like accelerogram is much smaller than the same region of the ordinary one. It follows that most of the energy transmitted by a pulse-like accelerogram to a structure is concentrated in a small interval. This is also evident when analyzing the one-sided *EPSD* functions plotted in Fig. 6. These functions present discontinuities of first kind at time instant $t = t_k$, $k = 1,2, \ldots,5$ (see Eq. (14)). To avoid numerical errors, it is appropriate to select $t_{k-1}, t_k \neq t_{a_s}$.

4.2.3. Fully non-stationary samples

In the previous sections, the parameters characterizing the *EPSD* function are determined. In this section, two sets of samples of fully non-stationary zero-mean Gaussian stochastic processes are estimated in such a way that the selected accelerogram can be considered as one of its own samples. According to the procedure described in Ref. [51], the two sets of $N_s = 10000$ samples have been generated as follows:

$$\ddot{U}_g^{(i)}(t) = a(t)\sqrt{2\Delta\omega}\left[\sum_{r=1}^{m_N}\sum_{k=1}^{5}\mathbb{W}\left(t_{k-1}, t_k\right)\cos\left(r\Delta\omega t + \theta_r^{(i)}\right)\sqrt{G_{X_k}(r\Delta\omega)}\right]; \quad i = 1,2,\ldots,10000 \tag{50}$$

Here, it is assumed a frequency step $\Delta\omega = 2\pi/D$, an upper cut-off

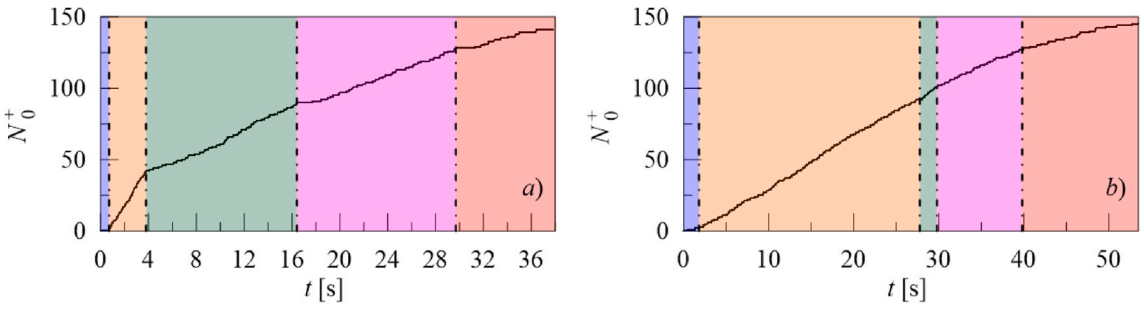

Fig. 3. Cumulative zero-level up-crossings functions of two target accelerograms together with the subdivision of the temporal region delineated by dashed black vertical lines: a) Imperial Valley-06 (pulse-like accelerogram); b) Imperial Valley-02 (ordinary accelerogram).

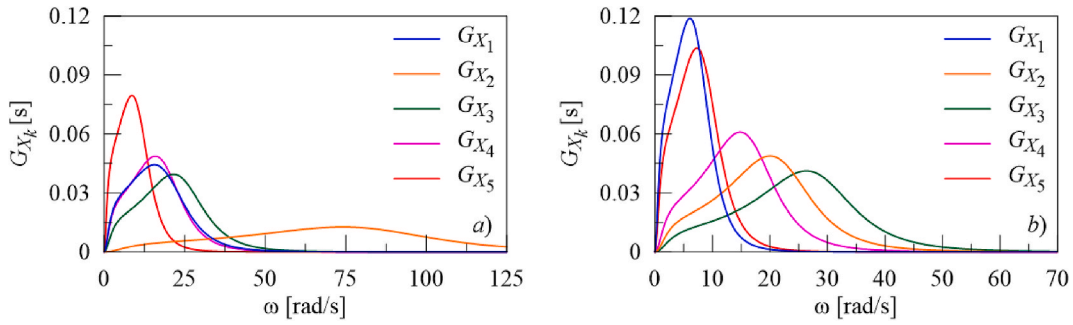

Fig. 4. One-sided *PSD* functions in the five contiguous time intervals of the selected accelerograms: a) Imperial Valley-06 (pulse-like accelerogram); b) Imperial Valley-02 (ordinary accelerogram).

Table 1
Main parameters of the one-sided *PSD* functions of the target pulse-like accelerogram of Imperial Valley-06.

k	t_k [s]	ΔT_k [s]	N_k^+	P_k	Ω_k [rad/s]	ρ_k [rad/s]	ω_{Hk} [rad/s]	ω_{Lk} [rad/s]	β_k
1	0.7	0.7	2	12	18.081	12.694	1.808	28.236	7.277
2	3.8	3.1	40	61	81.204	37.153	8.120	110.927	20.824
3	16.4	12.6	48	92	23.945	12.560	2.395	33.993	7.0779
4	29.7	13.3	38	103	17.958	10.792	1.796	26.592	6.125
5	37.86	8.16	13	87	10.010	7.114	1.001	15.701	4.082

Table 2
Main parameters of the one-sided *PSD* functions of the target ordinary accelerogram of Imperial Valley-02.

k	t_k [s]	ΔT_k [s]	N_k^+	P_k	Ω_k [rad/s]	ρ_k [rad/s]	ω_{Hk} [rad/s]	ω_{Lk} [rad/s]	β_k
1	1.81	1.81	2	8	6.981	4.610	0.698	10.670	2.632
2	27.77	25.96	90	128	21.791	9.454	2.179	29.355	5.290
3	29.78	2.01	9	11	28.274	10.640	2.827	36.786	5.937
4	39.80	10.02	26	43	16.320	7.884	1.632	22.627	4.427
5	53.45	13.65	18	54	8.286	5.127	0.829	12.387	2.915

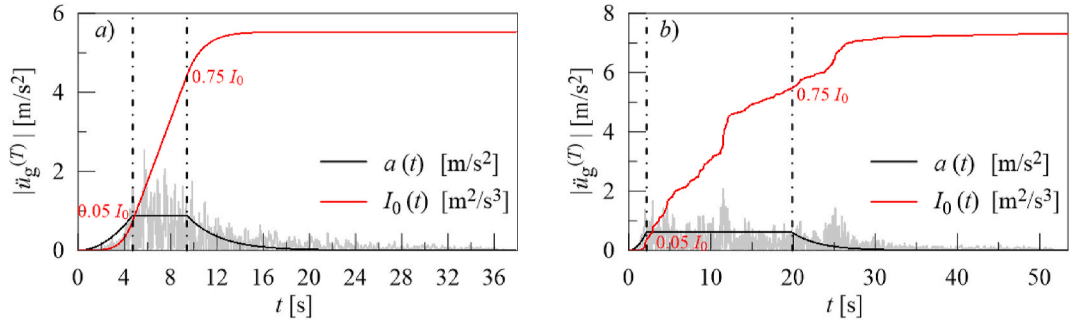

Fig. 5. Comparison between the absolute values of the target accelerogram (grey line), its cumulative intensity function $I_0(t)$, and the modulating function $a(t)$ together with the indication of the target $D_{5\text{-}75}$ delimited by two vertical lines: a) Imperial Valley-06 (pulse-like accelerogram); b) Imperial Valley-02 (ordinary accelerogram).

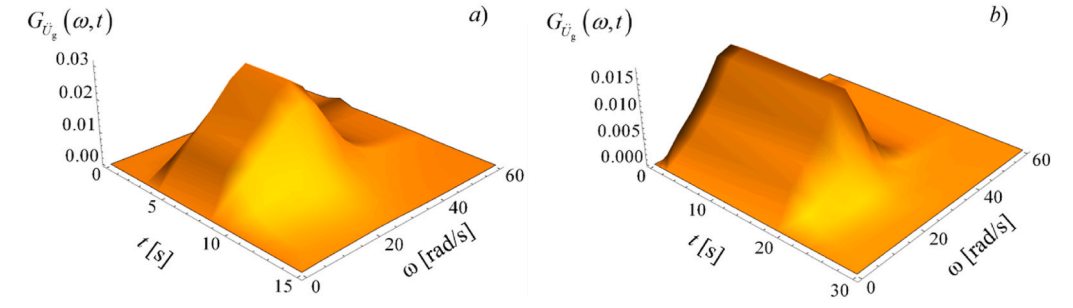

Fig. 6. Joint time-frequency representation of the one-sided *EPSD* functions [m²/s³]: a) Imperial Valley-06 (pulse-like accelerogram); b) Imperial Valley-02 (ordinary accelerogram).

circular frequency $\omega_N = \pi/\Delta t$ and a number of discrete frequencies $m_N = \omega_N/\Delta\omega$. In Eq. (50) the random phase angle, $\theta_r^{(i)}$, is uniformly distributed over the interval $[0, 2\pi]$. Once the samples of artificial accelerograms are generated, the main statistics of the structural response can be evaluated by applying the *MCS*.

The number of samples N_s was selected to ensure that the estimated statistical quantities (i.e. mean and variance) stabilize within an acceptable tolerance.

In Fig. 7 are compared the cumulative intensity function of the target accelerograms $I_0(t)$ (red line) and those obtained by means of *MCS*. In particular, the grey area defines the envelope of the cumulative intensity functions computed for each set of N_s samples of artificial accelerograms; the black line defines the corresponding mean value trends $\bar{I}_0(t)$; the confidence interval (computed as the mean value plus/minus one standard deviation σ of the data) is represented with a dashed black line. On the time axis, the time interval corresponding to the strong motion duration $D_{5\text{-}75}$ of the target motions is also identified by the two vertical lines. From Fig. 7, it is apparent that, within the strong motion duration, a general very good agreement is obtained between the cumulative intensity of the target accelerogram (hereafter referred as target intensity), and the mean trend of the intensity functions computed for the N_s samples of artificial accelerograms. For the two cases, the final (cumulative) values of the computed mean value intensities $\bar{I}_0$ are coincident with the total intensity I_0 of two target accelerograms.

The comparison between the target function and the mean trends computed for set of N_s artificial accelerograms is also presented in Fig. 8, in terms of cumulative zero-level up-crossings. It can be observed that, for the entire duration of the signal, there is a very good agreement between the trends of the zero-level up-crossings computed for the two target accelerograms $N_0^+(t)$ and the mean value trends $\overline{N}_0^+(t)$ evaluated for the two sets of samples of the artificial accelerograms.

4.3. SDoF systems

Four different *SDoF* systems have been considered herein to validate the procedure proposed in Section 3 by comparing the time variant *NGSMs*, assessed through the proposed analytical approach with those obtained with the *MCS*. The natural periods of the oscillators, with unit mass, have been assumed as: $T_0 = 0.2$ s, $T_0 = 0.4$ s, $T_0 = 0.6$ s, $T_0 = 1$ s; and the damping ratio is set equal to $\xi_0 = 0.05$.

The time histories of the main *NGSMs* of the response: $\lambda_{0,u}(t)$, $\mathrm{Re}\{\lambda_{1,u}(t)\}$, $\lambda_{2,u}(t)$ of the four oscillators, adopting the proposed approach, are depicted in Figs. 9–11 with black lines, and compared with the analogous functions obtained by *MCS* using *Ns* = 10000 samples, depicted in Figs. 9–11 by red dots, and evaluated using the procedure described in Ref. [41].

It is useful to remember that the one-sided *EPSD* function defined in Eq. (14) presents discontinuity of the first kind at time instant $t = t_k$, $k = 1,2, \ldots, n$, while the *modulating function* is piecewise defined at time instant $t = t_{a_1}, t_{a_2}$. Note that, especially for pulse-like accelerograms, possible numerical errors in the evaluation of *NGSMs* have been avoided because it has been chosen $t_{k-1}, t_k \neq t_{a_s}$.

Upon analyzing the *NGSMs* reported in Figs. 9–11, it becomes evident that there is a notable consistency between the functions derived by the proposed method (black lines) and those obtained through *MCS* (red dots). The trends observed for both accelerograms highlight the robustness and agreement between the outcomes achieved by these distinct methods. Moreover, examining these figures, it becomes evident that even though the ordinary accelerogram (Imperial Valley-02 (ELC270)) possesses a total intensity greater than the pulse-like accelerogram (Imperial Valley-06 (HVP225)), the maxima of all spectral moments for the pulse-like accelerogram are greater than the maxima of the ordinary accelerogram. This is a consequence of the concentration of the energy for pulse-like accelerograms in a smaller temporal interval.

4.4. MDoF system

After characterizing the ground motion acceleration process, the subsequent step in structural engineering involves assessing the structural response to predict the safety of structural systems.

This section illustrates the usefulness of the time-variant *NGSMs*, obtained through the proposed analytical approach, in assessing the structural reliability of a multi-degree-of-freedom linear system (*MDoF*) under fully non-stationary zero-mean Gaussian stochastic excitations. In the framework of stochastic dynamics, the problem of probabilistically predicting the time instant in which the extreme value of the response, at a critical location, exits for the first time from a prescribed safe domain is termed *first passage problem*. Unfortunately, this problem can be only solved numerically or in approximate form [see e.g., 20, 21,22,45]. In particular, the extreme value random response process of the selected structural response of interest $Y(t)$ is introduced as:

$$Y_{\max}(t) = \max_{0\le\tau\le t} |Y(\tau)| \tag{51}$$

and according to the approximation proposed by Corotis et al. [45], the reliability function is evaluated as follows:

$$\begin{aligned} L_{Y_{\max}}(b,t) &= \Pr\langle Y_{\max}(t) \le b \mid Y_{\max}(0) < b\rangle \\ &\approx L_{Y_{\max}}(b,0)\exp\left[-\int_0^t \eta_Y(b,\rho)\,\mathrm{d}\rho\right] \end{aligned} \tag{52}$$

where $L_{Y_{\max}}(b,0)$ is the reliability at time $t = 0$, which for quiescent structural systems is unitary, and $\eta_Y(b,t)$ is the so-called hazard function defined as:

$$\eta_Y(b,t) = \frac{1}{\pi}\sqrt{\frac{\lambda_{2,Y}(t)}{\lambda_{0,Y}(t)}}\left[\frac{1-\exp\left(-b\,\delta_Y(t)\sqrt{\frac{\pi}{2\,\lambda_{0,Y}(t)}}\right)}{\exp\left(\frac{b^2}{2\,\lambda_{0,Y}(t)}\right)-1}\right] \tag{53}$$

where $\delta_Y(t)$ is the bandwidth parameter, which in the non-stationary

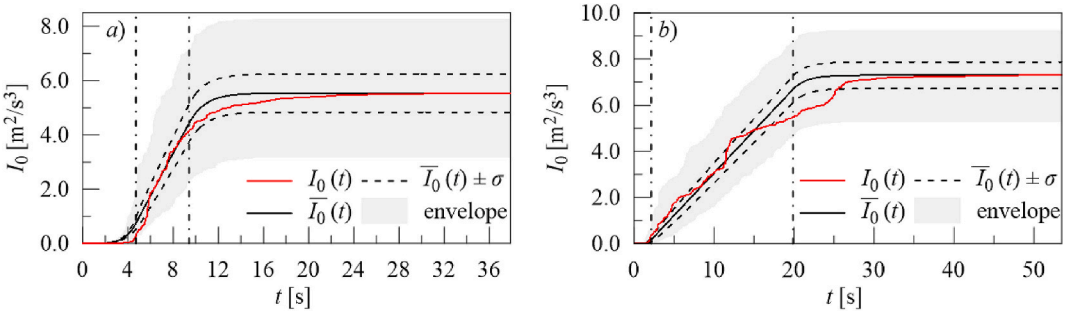

Fig. 7. Cumulative intensity functions of the target motion and of the set of artificial accelerograms together with the indication of the target $D_{5\text{-}75}$ delimited by two vertical lines: a) Imperial Valley-06 (pulse-like accelerogram); b) Imperial Valley-02 (ordinary accelerogram).

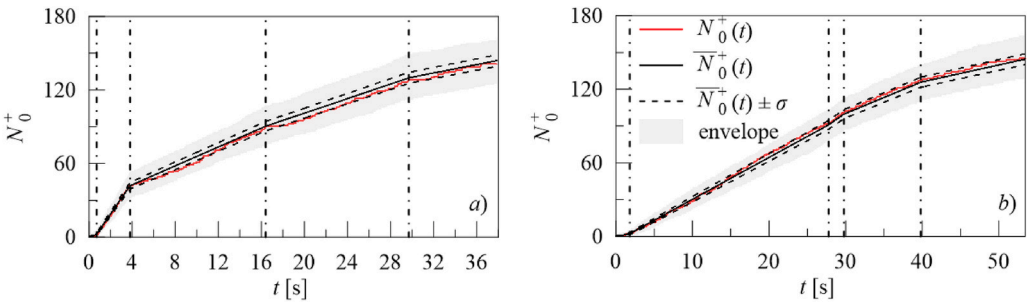

Fig. 8. Cumulative zero-level up-crossings functions of the target motion and of the set of artificial accelerograms together with the subdivision of the temporal region delineated by dashed black vertical lines: a) Imperial Valley-06 (pulse-like accelerogram); b) Imperial Valley-02 (ordinary accelerogram).

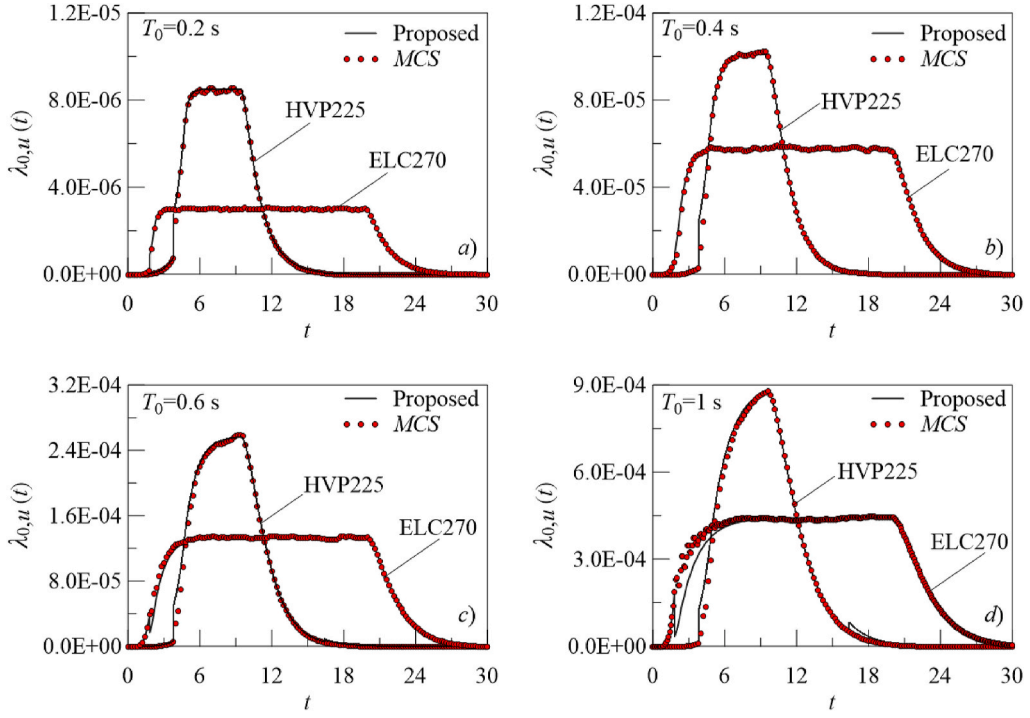

Fig. 9. Comparison between the time-variant histories of the $\lambda_{0,u}(t)$ *NGSMs* [m^2] of the relative to ground floor displacement, evaluated by applying the proposed analytical solution and the *MCS* considering both the pulse-like Imperial Valley-06 (HVP225) and the ordinary Imperial Valley-02 (ELC270) accelerograms as target ones.

case, has been defined as [26,27]:

$$\delta_Y(t) = \sqrt{1 - \frac{\mathrm{Re}\{\lambda_{1,Y}(t)\}^2}{\lambda_{0,Y}(t)\,\lambda_{2,Y}(t)}} \tag{54}$$

Once the reliability function is derived, the mean value of the largest peak can be evaluated as follow [20,21]:

$$\mu_{Y_{\max}}(t) = \int_0^b Y_{\max}(t)\,\frac{\partial L_{Y_{\max}}(\rho,t)}{\partial \rho}\,\mathrm{d}\rho \tag{55}$$

To demonstrate the effectiveness of the proposed procedure, a classically damped linear *MDoF* system with irregular distributions of mass and stiffness in plan and elevation has been selected as case study. The system is composed of a six-story spatial frame with inter-storey height of $h = 3$ m and the 3D-frame is modeled as a 18-DoF system. The first four storeys have dimensions of 25 m × 10 m, which reduce to 13 m × 10 m for the last two storeys (see Fig. 12). The layout of the floors, along with the orientation of the columns, is sketched in Fig. 13. The dimensions of the beams and columns vary along the height of the building: the beams are 30 × 70 cm on the first two storeys, 30 × 60 cm on the third and fourth storeys, and 30 × 50 cm on the last two storeys. The columns range from 30 × 70 to 30 × 40 cm on the first four storeys and are 30 × 30 cm on the last two storeys. The first five periods of vibration are as follows: $T_1 = 0.548$ s, $T_2 = 0.509$ s, $T_3 = 0.347$ s, $T_4 = 0.243$ s, $T_5 = 0.242$ s. A constant viscous damping ratio $\xi_0 = 0.05$ is assumed for all modes of vibration.

The spatial frame is subjected to the pulse-like accelerogram analyzed in section 4.2: the first horizontal component (HVP225) of the 1979 "Imperial Valley-06" ground motion. It is assumed that the ground motion is in the x-direction. It follows that the attention is focused on the displacements of the barycenter of the first floor in the same direction. In Figs. 14–16, the time histories of the *NGSMs* obtained by the proposed formulation are depicted and compared with the results of the *MCS* (10000 samples).

Upon examination of the *NGSMs* depicted in Figs. 14–16, it is apparent that a significant coherence exists between the functions generated by the proposed method (depicted as black lines) and those obtained through *MCS* (represented by red dots). The observed patterns underscore the robustness and alignment of outcomes between these

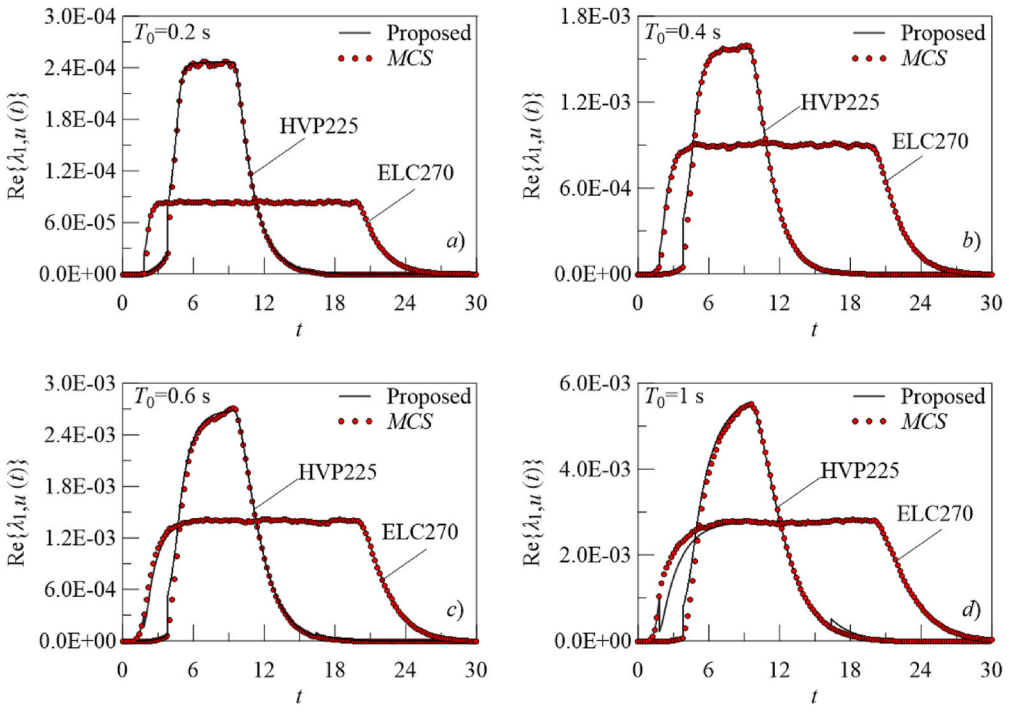

Fig. 10. Comparison between the time-variant histories of the real part of $\lambda_{1,u}(t)$ *NGSMs* [m^2/s] of the relative to ground floor displacement, evaluated by applying the proposed analytical solution and the *MCS* considering both the pulse-like Imperial Valley-06 (HVP225) and the ordinary Imperial Valley-02 (ELC270) accelerograms as target ones.

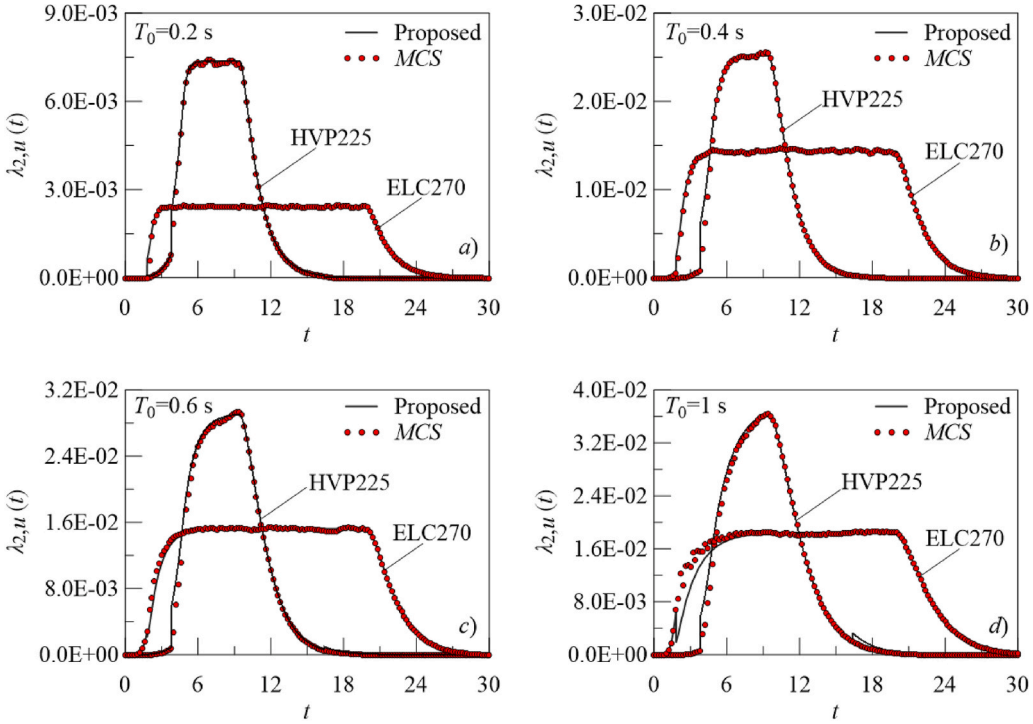

Fig. 11. Comparison between the time-variant histories of $\lambda_{2,u}(t)$ *NGSMs* [m^2/s^2] of the relative to ground floor displacement, evaluated by applying the proposed analytical solution and the *MCS* considering both the pulse-like Imperial Valley-06 (HVP225) and the ordinary Imperial Valley-02 (ELC270) accelerograms as target ones.

distinct methodologies.

In order to validate the procedure previously described, the formulation has been implemented for the prediction of the mean value of the largest peak of the response $\mu_{Y_{\max}}(t)$. In Fig. 17, the mean value of the response $\mu_{Y_{\max}}(t)$ has been evaluated, using the Corotis et al. [45] model, and the result has been compared with the *MCS* based on 10000 samples. It is evident that the two trends closely align for the initial 7 s. After almost 10 s, the spectral moments decrease, and consequently, the mean

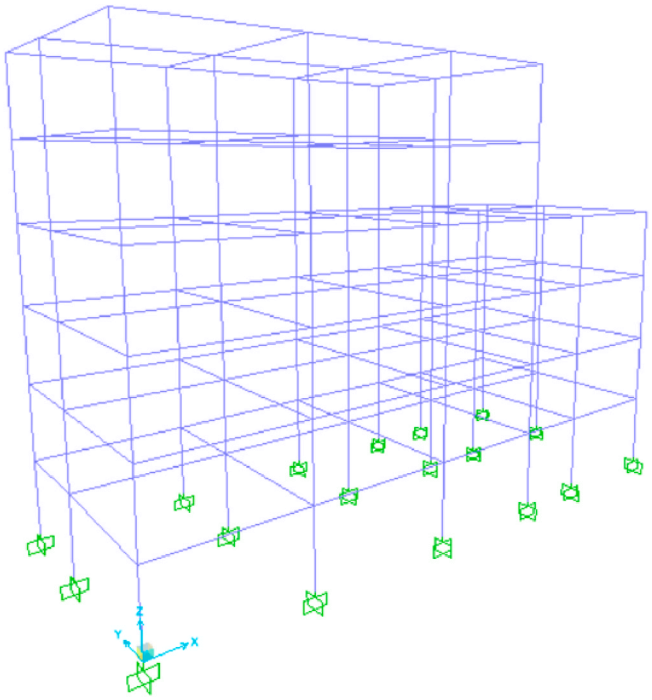

Fig. 12. Six-story frame structure.

value of the largest peak remains constant. The maximum difference between the results obtained with the proposed analytical solution and those obtained with *MCS* is 2.47%.

5. Conclusions

In the probabilistic analysis of structural systems under seismic excitation, evaluating the spectral characteristics of both the input ground acceleration and the structural response is essential. Within this context, this paper introduces an innovative method to derive the spectral characteristics of the response of linear structural systems subjected to seismic acceleration modeled as stochastic processes. To do this explicit closed-form solutions of modal and nodal one-sided *evolutionary power spectral density* (*EPSD*) functions of structural response are first evaluated. These closed-form solutions are computed using a novel model of the one-sided (*EPSD*) function of the zero-mean Gaussian input process, recently proposed by the authors. This model, employed to generate artificial accelerograms so that a target accelerogram is considered as one of its own samples, is hereby extended to include the use of pulse-like accelerograms as the target signals. This extension involves: *i*) partitioning the selected target accelerogram into multiple time intervals, determined by variations in slope changes of the cumulative zero-level up-crossings function, each containing at least one zero-level up-crossing and peak; *ii*) assessing a one-sided *PSD* function of a stationary sub-process for each time interval into which the target motion has been subdivided. Once the one-sided *EPSD* function of the input process is defined, a procedure is proposed to evaluate the explicit closed-form solution of the time-frequency varying response function of linear structural systems and consequently the one-sided *EPSD* function of the responses.

Then, the time variation of the non-geometric spectral moments *NGSMs*, useful for performing the safety assessment of linear structures, are evaluated by numerical integrations. In order to evidence the effectiveness of the proposed procedure, the spectral characteristics of the structural response of four single-degree-of-freedom systems and a six-story spatial frame are evaluated and compared with the results

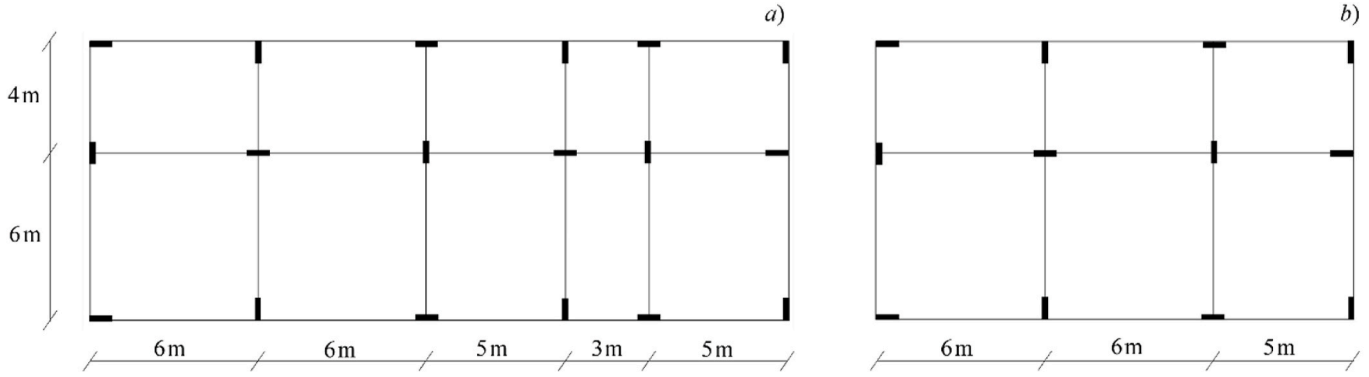

Fig. 13. a) Bottom and b) top plan layouts of the building.

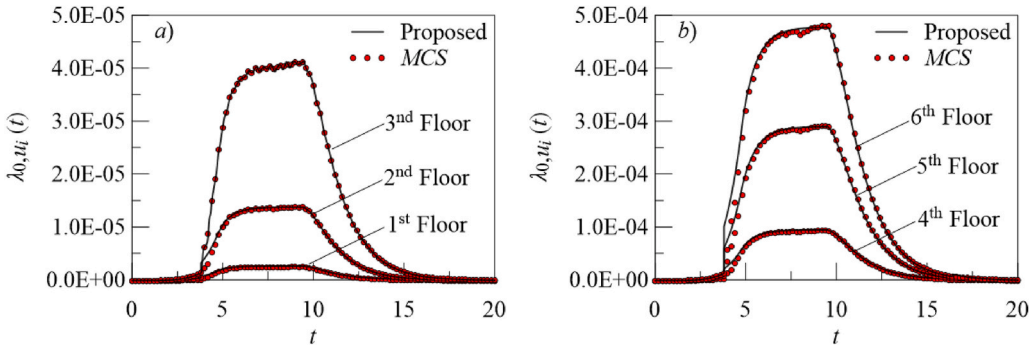

Fig. 14. Comparison between the time-variant histories of the $\lambda_{0,tii}(t)$ *NGSMs* [m^2], of the six relative to ground floor displacements, evaluated by applying the proposed analytical solution and the *MCS* considering the Imperial Valley-06 (pulse-like accelerogram) as target motion in the fully non-stationary input process: a) first three floors; b) last three floors.

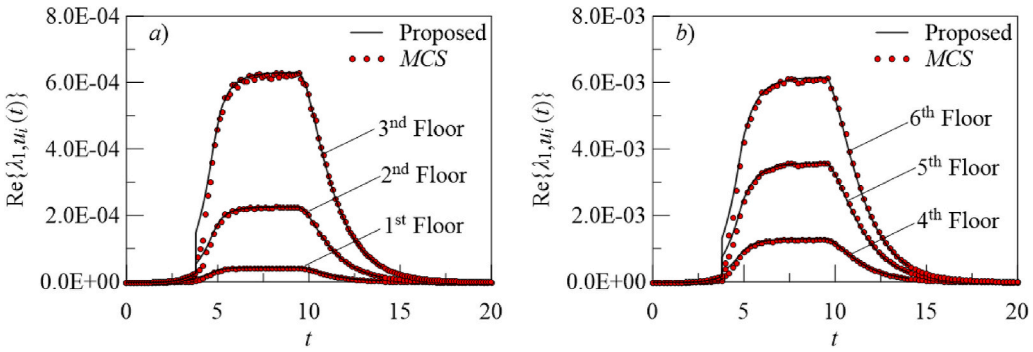

Fig. 15. Comparison between the real part of the time-variant histories of the $\lambda_{1,ui}(t)$ *NGSMs* [m^2/s], of the six relative to ground floor displacements, evaluated by applying the proposed analytical solution and the *MCS* considering the Imperial Valley-06 (pulse-like accelerogram) as target motion in the fully non-stationary input process: a) first three floors; b) last three floors.

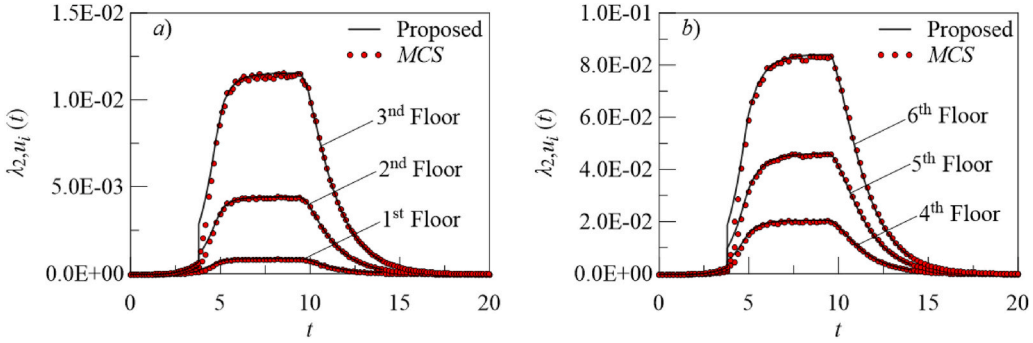

Fig. 16. Comparison between the time-variant histories of the $\lambda_{2,ui}(t)$ *NGSMs* [m^2/s^2], of the six relative to ground floor displacements, evaluated by applying the proposed analytical solution and the *MCS* considering the Imperial Valley-06 (pulse-like accelerogram) as target motion in the fully non-stationary input process: a) first three floors; b) last three floors.

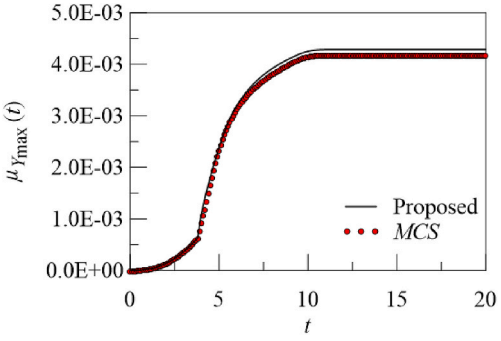

Fig. 17. Comparison between the mean value of the response [m] obtained by adopting the proposed formulation (black line) and the *MCS* (red dots).

obtained using the Monte Carlo simulation technique.

CRediT authorship contribution statement

Federica Genovese: Writing – original draft, Validation, Software, Methodology, Investigation, Formal analysis, Data curation, Writing – review & editing. **Giuseppe Muscolino:** Writing – review & editing, Writing – original draft, Visualization, Supervision, Methodology, Investigation, Conceptualization.

Declaration of competing interest

The authors declare that they have no known competing financial interests or personal relationships that could have appeared to influence the work reported in this paper.

Data availability

Data will be made available on request.

References

[1] K.K. Yadav, V.K. Gupta, Near-fault fling-step ground motions: characteristics and simulation, Soil Dynam. Earthq. Eng. 101 (2017) 90–104, https://doi.org/10.1016/j.soildyn.2017.06.022.
[2] G.W. Housner, M.D. Trifunac, Analysis of accelerograms—parkfield earthquake, Bull. Seismol. Soc. Am. 57 (6) (1967) 1193–1220, https://doi.org/10.1785/BSSA0570061193.
[3] S. Bhagat, A.C. Wijeyewickrema, N. Subedi, Influence of near-fault ground motions with fling-step and forward-directivity characteristics on seismic response of base-isolated buildings, J. Earthq. Eng. 25 (3) (2021) 455–474, https://doi.org/10.1080/13632469.2018.1520759.
[4] S. Mukhopadhyay, V.K. Gupta, Directivity pulses in near-fault ground motions—I: identification, extraction and modeling, Soil Dynam. Earthq. Eng. 50 (2013) 1–15, https://doi.org/10.1016/j.soildyn.2013.02.017.
[5] F. Vats, D. Basu, Alternate algorithm for characterization of strong velocity pulse in ground motions, Int. J. Adv. Eng. Sci. Appl. Math. (2023) 1–21.
[6] Z. Chang, F. De Luca, K. Goda, Automated classification of near-fault acceleration pulses using wavelet packets, Comput. Aided Civ. Infrastruct. Eng. 34 (7) (2019) 569–585.
[7] Z. Chang, Q. Gao, G. Monti, H. Yu, S. Yuan, Selection of pulse-like ground motions with strong velocity-pulses using moving-average filtering, Soil Dynam. Earthq. Eng. 164 (2023) 107574, https://doi.org/10.1016/j.soildyn.2022.107574.
[8] G. Chen, Y. Liu, M. Beer, Identification of near-fault multi-pulse ground motion, Appl. Math. Model. 117 (2023) 609–624, https://doi.org/10.1016/j.apm.2023.01.002.
[9] X. Chen, D. Wang, R. Zhang, Identification of pulse periods in near-fault ground motions using the HHT method, Bull. Seismol. Soc. Am. 109 (6) (2019) 2384–2398, https://doi.org/10.1785/0120190046.
[10] J. Feng, B. Zhao, T. Zhao, Quantitative identification of near-fault pulse-like ground motions based on variational mode decomposition technique, Soil Dynam. Earthq. Eng. 151 (2021) 107009, https://doi.org/10.1016/j.soildyn.2021.107009.
[11] B. Ghanbari, M. Fathi, Extraction of velocity pulses of pulse-like ground motions using empirical Fourier decomposition, J. Seismol. 26 (5) (2022) 967–986, https://doi.org/10.1007/s10950-022-10106-8.

[12] G.R. Saragoni, G.C. Hart, Simulation of artificial earthquakes, Earthq. Eng. Struct. Dynam. 2 (3) (1973) 249–267, https://doi.org/10.1002/eqe.4290020305.
[13] G.C. Marano, Non-stationary stochastic modulation function definition based on process energy release, Phys. Met.: Stat. Mech. 517 (2019) 280–289, https://doi.org/10.1016/j.physa.2018.08.039.
[14] J.P. Conte, B.F. Peng, Fully nonstationary analytical earthquake ground-motion model, J. Eng. Mech. 123 (1) (1997) 15–24, https://doi.org/10.1061/(ASCE)0733-9399(1997)123:1(15.
[15] S. Rezaeian, A. Der Kiureghian, A stochastic ground motion model with separable temporal and spectral nonstationarities, Earthq. Eng. Struct. Dynam. 37 (13) (2008) 1565–1584, https://doi.org/10.1002/eqe.831.
[16] M.B. Priestley, Evolutionary spectra and non-stationary processes, J. R. Stat. Soc., Ser. B, Methodol. 27 (2) (1965) 204–229, https://doi.org/10.1111/j.2517-6161.1965.tb01488.x.
[17] G. Stefanou, S. Tsiliopoulos, Estimation of evolutionary power spectra of seismic accelerograms, in: M. Papadrakakis, M. Fragiadakis (Eds.), 7th International Conference on Computational Methods in Structural Dynamics and Earthquake Engineering, vol. 3, 2019, pp. 5880–5888, https://doi.org/10.7712/120119.7353.20116.
[18] G. Muscolino, F. Genovese, G. Biondi, E. Cascone, Generation of fully non-stationary random processes consistent with target seismic accelerograms, Soil Dynam. Earthq. Eng. 141 (2021) 106467, https://doi.org/10.1016/j.soildyn.2020.106467.
[19] F. Genovese, G. Biondi, E. Cascone, G. Muscolino, Energy-compatible modulating functions for the stochastic generation of fully non-stationary artificial accelerograms and their effects on seismic site response analysis, Earthq. Eng. Struct. Dynam. (2023) 1–25, https://doi.org/10.1002/eqe.3889.
[20] L.D. Lutes, S. Sarkani, Stochastic Analysis of Structural and Mechanical Vibrations, Prentice-Hall, Upper Saddle River, 1997.
[21] J. Li, J.B. Chen, Stochastic Dynamics of Structures, John Wiley & Sons, Singapore, 2009.
[22] E.H. Vanmarcke, Properties of spectral moments with applications to random vibrations, J. Eng. Mech. 98 (1972) 425–446, https://doi.org/10.1061/JMCEA3.0001593.
[23] E.H. Vanmarcke, On the distribution of the first-passage time for normal stationary random processes, J. Appl. Mech. 42 (1975) 215–2205, https://doi.org/10.1115/1.3423521.
[24] M. Di Paola, Transient Spectral Moments of Linear Systems, SM Arch, vol. 10, 1985, pp. 225–243.
[25] G. Muscolino, Nonstationary envelope in random vibration theory, J. Eng. Mech. 114 (1988) 1396–1413, https://doi.org/10.1061/(ASCE)0733-9399(1988)114:8(1396.
[26] G. Michaelov, S. Sarkani, L.D. Lutes, Spectral characteristics of nonstationary random processes -A critical review, Struct. Saf. 21 (1999) 223–244, https://doi.org/10.1016/S0167-4730(99)00022-3.
[27] G. Michaelov, S. Sarkani, L.D. Lutes, Spectral characteristics of nonstationary random processes – response of a simple oscillator, Struct. Saf. 21 (1999) 245–267, https://doi.org/10.1016/S0167-4730(99)00019-3.
[28] M. Di Paola, G. Petrucci, Spectral moments and pre-envelope covariances of nonseparable processes, J. Appl. Mech. 57 (1990) 218–224, https://doi.org/10.1115/1.2888307.
[29] G. Muscolino, Nonstationary pre-envelope covariances of non-classically damped systems, J. Sound Vib. 149 (1991) 107–123, https://doi.org/10.1016/0022-460X(91)90914-6.
[30] M. Barbato, J.P. Conte, Spectral characteristics of non-stationary random processes: theory and applications to linear structural models, Probabilist. Eng. Mech. 23 (2008) 416–426, https://doi.org/10.1016/j.probengmech.2007.10.009.
[31] S. Caddemi, G. Muscolino, Pre-envelope covariance differential equations for white and non-white input processes, Meccanica 33 (1998) 1–10, https://doi.org/10.1023/A:1004261032261.
[32] R.S. Langley, Structural response to non-stationary non-white stochastic ground motion, Earthq. Eng. Struct. Dynam. 14 (1986) 909–924, https://doi.org/10.1002/eqe.4290140607.
[33] G. Borino, M. Di Paola, G. Muscolino, Non-stationary spectral moments of base excited MDOF systems, Earthq. Eng. Struct. Dynam. 16 (1988) 745–756, https://doi.org/10.1002/eqe.4290160509.
[34] S. Caddemi, P. Colajanni, I. Duca, G. Muscolino, Non-geometric spectral moments for frequency varying filtered input processes, Probabilist. Eng. Mech. 19 (2004) 21–31, https://doi.org/10.1016/j.probengmech.2003.11.003.
[35] N.C. Nigam, Introduction to Random Vibrations, M1T Press, London, 1983.
[36] J.P. Conte, B.-F. Peng, An explicit closed-form solution for linear systems subjected to nonstationary random excitation, Probabilist. Eng. Mech. 11 (1996) 37–50, https://doi.org/10.1016/0266-8920(95)00026-7.
[37] B.-F. Peng, J.P. Conte, Closed-form solutions for the response of linear systems to fully nonstationary earthquake excitation, J. Eng. Mech. 124 (1998) 684–694, https://doi.org/10.1061/(ASCE)0733-9399(1998)124:6(684.
[38] R.S. Jangid, Response of SDOF system to non-stationary earthquake excitation, Earthq. Eng. Struct. Dynam. 33 (2004) 1417–1428, https://doi.org/10.1002/eqe.409.
[39] M. Barbato, M. Vasta, Closed-form solutions for the time-variant spectral characteristics of nonstationary random processes, Probabilist. Eng. Mech. 25 (2010) 9–17, https://doi.org/10.1016/j.probengmech.2009.05.002.
[40] Q.Y. Cao, S.L.J. Hu, H.J. Li, Evaluating response of simple oscillators to a particular kind of time–frequency non-separable evolutionary stochastic processes, Probabilist. Eng. Mech. 61 (2020) 103076, https://doi.org/10.1016/j.probengmech.2020.103076.
[41] G. Muscolino, T. Alderucci, Closed-form solutions for the evolutionary frequency response function of linear systems subjected to separable or non-separable non-stationary stochastic excitations, Probabilist. Eng. Mech. 40 (1) (2015) 75–89, https://doi.org/10.1016/j.probengmech.2015.02.001.
[42] T. Alderucci, G. Muscolino, Time–frequency varying response functions of non-classically damped linear structures under fully non-stationary stochastic excitations, Probabilist. Eng. Mech. 54 (2018) 95–109, https://doi.org/10.1016/j.probengmech.2017.08.004.
[43] F. Genovese, T. Alderucci, G. Muscolino, Design sensitivity analysis of structural systems with damping devices subjected to fully non-stationary stochastic seismic excitations, Comput. Struct. 284 (2023) 107067, https://doi.org/10.1016/j.compstruc.2023.107067.
[44] T. Alderucci, G. Muscolino, Fully nonstationary analysis of linear structural systems subjected to multicorrelated stochastic excitations, ASCE ASME J. Risk Uncertain. Eng. Syst. A Civ. Eng. 2 (2) (2016) C4015007, https://doi.org/10.1061/AJRUA6.0000842.
[45] R.B. Corotis, E.H. Vanmarcke, C.A. Cornell, First passage of non-stationary random processes, J. Eng. Mech. 98 (1972) 401–414, https://doi.org/10.1061/JMCEA3.0001591.
[46] J.-N. Yang, Non-Stationary envelope process and first excursion probability, J. Struct. Mech. 1 (1972) 231–248.
[47] R.S. Langley, A first passage approximation for normal stationary random process, J. Sound Vib. 122 (1988) 261–275, https://doi.org/10.1016/S0022-460X(88)80353-5.
[48] M. Barbato, J.P. Conte, Structural reliability applications of nonstationary spectral characteristics, J. Eng. Mech. 137 (2011) 371–382, https://doi.org/10.1061/(ASCE)EM.1943-7889.0000238.
[49] M. Barbato, J.P. Conte, Time-variant reliability analysis of linear elastic systems subjected to fully nonstationary stochastic excitations, J. Eng. Mech. 141 (2015) 04014173, https://doi.org/10.1061/(ASCE)EM.1943-7889.0000895, 1-10.
[50] T. Alderucci, G. Muscolino, S. Urso, Stochastic analysis of linear structural systems under spectrum and site intensity compatible fully non-stationary artificial accelerograms, Soil Dynam. Earthq. Eng. 126 (2019) 105762, https://doi.org/10.1016/j.soildyn.2019.105762.
[51] M. Shinozuka, Y. Sato, Simulation of nonstationary random processes, J. Eng. Mech. 93 (1) (1967) 11–40, https://doi.org/10.1061/JMCEA3.0000822.
[52] P.C. Jennings, G.W. Housner, C. Tsai, Simulated earthquake motions for design purpose, Proc. 4th World Conference Earthquake Engineering A-1 (1969) 145–160. Santiago.
[53] P. Spanos, G.P. Solomos, Markov approximation to transient vibration, J. Eng. Mech. 109 (1983) 1134–1150.
[54] T.I. Hsu, M.C. Bernard, A random process for earthquake simulation, Earthq. Eng. Struct. Dynam. 6 (4) (1978) 347–362.
[55] M.D. Trifunac, A.D. Brady, A study of the duration of strong earthquake ground motion, Seismol. Soc. Am. 65 (3) (1975) 581–626, https://doi.org/10.1785/BSSA0650030581.
[56] J. Lin, W. Zhang, F.W. Williams, Pseudo-excitation algorithm for nonstationary random seismic responses, Eng. Struct. 16 (4) (1994) 270–276, https://doi.org/10.1016/0141-0296(94)90067-1.
[57] L. Meirovitch, Principles and Techniques of Vibrations, Prentice Hall, 1997.
[58] R.R. Craig, A.J. Kurdila, Fundamentals of Structural Dynamics, John Wiley & Sons, 2006.
[59] R.W. Clough, J. Penzien, Dynamics of Structures, McGraw Hill, New York, 1993.
[60] G. Borino, G. Muscolino, Mode-superposition methods in dynamic analysis of classically and non-classically damped linear systems, Earthq. Eng. Struct. Dynam. 14 (5) (1986) 705–717, https://doi.org/10.1002/eqe.4290140503.
[61] G. Muscolino, Dynamically modified linear structures: deterministic and stochastic response, J. Eng. Mech. 122 (11) (1996) 1044–1051, https://doi.org/10.1061/(ASCE)0733-9399(1996)122:11(1044.
[62] EC8-1. EN 1998-1, Eurocode 8: Design of Structures for Earthquake Resistance - Part 1, 2003, 2003.